

# The Power of Linear Recurrent Neural Networks

**Frieder Stolzenburg**

FSTOLZENBURG@HS-HARZ.DE

**Sandra Litz**

*Department of Automation and Computer Sciences, Harz University of Applied Sciences, 38855 Wernigerode, Germany*

**Olivia Michael**

**Oliver Obst**

O.OBST@WESTERNSYDNEY.EDU.AU

*Centre for Research in Mathematics and Data Science, Western Sydney University, Penrith NSW 2751, Australia*

## Abstract

Recurrent neural networks are a powerful means to cope with time series. We show how linear, i.e., linearly activated recurrent neural networks (LRNNs) can approximate any time-dependent function  $f(t)$  given by a number of function values. The approximation can effectively be learned by simply solving a linear equation system; no backpropagation or similar methods are needed. Furthermore, the size of an LRNN can be reduced significantly in one step, after inspecting the eigenvalues of the network transition matrix, by taking only the most relevant components. Therefore, in contrast to others, we do not only learn network weights but also the network architecture. LRNNs have interesting properties: They end up in ellipse trajectories in the long run and allow the prediction of further values and compact representations of functions. We demonstrate this by several experiments, among them multiple superimposed oscillators (MSO), robotic soccer, and predicting stock prices. LRNNs outperform the previous state-of-the-art for the MSO task with a minimal number of units.

**Keywords:** recurrent neural network; linear activation; time-series analysis; prediction; dimensionality reduction; approximation theorem; ellipse trajectories.

**MSC class:** 15A06 · **ACM class:** I.2.6

## 1. Introduction

Deep learning in general means a class of machine learning algorithms that use a cascade of multiple layers of nonlinear processing units for feature extraction and transformation (Deng and Yu, 2014). The tremendous success of deep learning in diverse fields of artificial intelligence, such as computer vision and natural language processing, seems to depend on a bunch of ingredients: artificial, possibly recurrent neural networks (RNNs), with nonlinearly activated neurons, convolutional layers, and iterative training methods like backpropagation (Goodfellow et al., 2016). But which of these components are really essential for machine learning tasks such as time-series analysis?

Research in time series analysis and hence modeling dynamics of complex systems has a long tradition and is still highly active due to its crucial role in many real-world applications (Lipton et al., 2015) like weather forecast, stock quotations, comprehension of trajectories of objects and agents, or solving number puzzles (Ragni and Klein, 2011; Glüge and Wendumuth, 2013). The analysis of time series allows, among others, data compression, i.e.,

compact representation of time series, e.g., by a function  $f(t)$ , and prediction of further values.

Numerous research addresses these topics by RNNs, in particular variants of networks with long short-term memory (LSTM) (Hochreiter and Schmidhuber, 1997). In the following, we consider an alternative, simple, yet very powerful type of RNNs: linear recurrent neural networks (LRNNs). Thus we only use linear activation, which allows us to minimize the network size in one step, namely by inspecting the eigenvalues of the network transition matrix (cf. Section 4.3). Therefore, in contrast to others, we do not only learn network weights but also the network architecture.

The rest of this paper is structured as follows: First, we briefly review related works (Section 2). We then formally introduce LRNNs as a special and simple kind of RNNs together with their properties, including the general network dynamics and their long-term behavior (Section 3). Afterwards, learning LRNNs is explained (Section 4). It is a relatively straightforward procedure which allows network size reduction; no backpropagation or gradient-descent method is needed. We then discuss results and experiments (Section 5), before we end up with conclusions (Section 6).

## 2. Related Works

### 2.1 Echo State Networks

Echo state networks (ESNs) (Jaeger and Haas, 2004; Jaeger, 2007) play a significant role in RNN research as they provide an architecture and supervised learning principle for RNNs. They do so by driving a random, large, fixed RNN, called *reservoir* in this context, with the input signal which then induces in each neuron within this reservoir network a nonlinear response signal. They combine a desired output signal by a trainable linear combination of all response signals, allowing dimensionality reduction by so-called *conceptors* (Jaeger, 2014, 2017).

Xue et al. (2007) propose a variant of ESNs that work with several independent (de-coupled) smaller networks. ESN-style (random) initialization has been shown effective for training RNNs with Hessian-free optimization (Martens and Sutskever, 2011). The latter paper addresses the problem of how to effectively train recurrent neural networks on complex and difficult sequence modeling problems which may contain long-term data dependencies. This can also be done with LRNNs (cf. MSO benchmark, Section 5.1). Tiňo (2018) considers the effect of weight changes in linear symmetric ESNs on (Fisher) memory of the network. From a solely theoretical point of view, Couillet et al. (2016) investigate the asymptotic performance of linear ESNs.

### 2.2 Recurrent Neural Networks

Simple RNNs are proposed by Elman (1990). By allowing them to accept sequences as inputs and outputs rather than individual observations, RNNs extend the standard feedforward multilayer perceptron networks. As shown in many sequence modeling tasks, data points such as video frames, audio snippets, and sentence segments are usually highly related in time. This results in RNNs being used as the indispensable tools for modeling such temporal dependencies. Linear RNNs and some of their properties (like short-term memory) are

already investigated by White et al. (1994). Unfortunately, however, it can be a struggle to train RNNs to capture long-term dependencies (Bengio et al., 1994; Pascanu et al., 2013). This is due to the gradients vanishing or exploding during backpropagation, which in turn makes the gradient-based optimization difficult.

Nowadays, probably the most prominent and dominant type of RNNs are long short-term memory (LSTM) networks introduced by Hochreiter and Schmidhuber (1997). The expression “long short-term” refers to the fact that LSTM is a model for the short-term memory which can last for a long period of time. An LSTM is well-suited to classify, process and predict time series given time lags of unknown size. They were developed to deal with the exploding and vanishing gradient problem when training traditional RNNs (see above). A common LSTM unit is composed of a cell, an input gate, an output gate, and a forget gate. Each unit type is activated in a different manner, whereas in this paper we consider completely linearly activated RNNs.

Ollivier et al. (2015) suggest to use the “NoBackTrack” algorithm in RNNs to train its parameters. This algorithm works in an online, memoryless setting which therefore requires no backpropagation through time. It is also scalable, thus avoiding the large computational and memory cost of maintaining the full gradient of the current state with respect to the parameters, but it still uses an iterative method, namely gradient descent. In contrast to this and other related works, in this paper we present a method working with linearly activated RNNs that does not require backpropagation or similar procedures in the learning phase.

Hu and Qi (2017) propose a novel state-frequency memory (SFM) RNN, which aims to model the frequency patterns of the temporal sequences. The key idea of the SFM is to decompose the memory states into different frequency states. In doing so, they can explicitly learn the dependencies of both the low and high frequency patterns. As we will see (cf. Section 5.1), RNNs in general can easily learn time series that have a constant frequency spectrum which may be obtained also by Fourier analysis.

Voelker et al. (2019) propose a memory cell for recurrent neural networks that maintains information across long windows of time using relatively few resources, called Legendre memory unit (LMU). It is derived from the linear transfer function for a continuous-time history of its input signal across a sliding window, approximated by coupled differential equations, which can implicitly also be solved by LRNNs (cf. Remark 1). Carta et al. (2021) propose an approach to address memorization challenges in RNNs, which puts forward a way between the random encoding in the reservoir paradigm and the vanishing-gradient prone approach of fully-trained RNNs. The objective is to train memorization units to maximize their short-term memory capacity, employing linear autoencoder for sequences. In both cases, backpropagation is employed, which is not needed for LRNNs whose network size is reduced significantly in addition (cf. Section 4.3), thus addressing the topic of architecture learning.

Architecture learning, in particular neural network pruning, is investigated many times in the literature. An early survey on pruning algorithms for neural networks is given by Reed (1993). In more recent work, Lee et al. (2019) present a method that prunes irrelevant connections between neurons for a given task prior to training and is applicable to a variety of modern neural network models, resulting in sparse networks. Furthermore, Molchanov et al. (2019) propose a method that estimates the contribution of a neuron to the final loss and iteratively removes those with smaller scores. In contrast to this, for LRNNs, the

network architecture and hence its size is reduced in one step by analyzing the network transition matrix (cf. Section 4.3).

### 2.3 Autoregression

An *autoregressive model* is a representation of a type of random process (Akaike, 1969). It specifies that the output variable or a vector thereof depends linearly on its own previous values and on a stochastic term (white noise). In consequence, the model is in the form of a stochastic differential equation as in general (physical) dynamic systems (Colonius and Kliemann, 2014). An LRNN is also linearly activated, but its output does not only depend on its own previous values and possibly white noise but on the complete state of the possibly big reservoir whose dynamics is explicitly dealt with. In addition, the size of the network might be reduced in the subsequent process. We will continue the comparison between autoregression and LRNNs later (in Sections 4.1 and 5.4).

Autoregressive frameworks are common in current machine-learning applications like language modeling, e.g., in the generative pre-trained transformer GPT-3, by next word prediction (Brown et al., 2020). The model applied in this context, however, is very complex (175 billion parameters) and non-linear. Related to autoregression is autoencoding of sequences. For this, Pasa and Sperduti (2014) show that linear autoencoders can be used for pre-training of RNNs, while we establish completely linear RNNs here. Furthermore, Sperduti (2006) gives an exact closed-form solution for the weights of the linear autoencoder, which is related to the approximation theorem for LRNNs (cf. Property 7).

## 3. Linear Recurrent Neural Networks

RNNs often host several types of neurons, each activated in a different manner (Elman, 1990; Hochreiter and Schmidhuber, 1997). In contrast to this, we here simply understand a homogeneous interconnected group of standard neurons as a neural network which may have arbitrary loops, akin to biological neuronal networks. We adopt a *discrete time model*, i.e., input and output can be represented by a time series and is processed stepwise by the network.

**Definition 1** (time series). A *time series* is a series of data points in  $d$  dimensions  $S(0), \dots, S(n) \in \mathbb{R}^d$  where  $d \geq 1$  and  $n \geq 0$ .

**Definition 2** (recurrent neural network). A *recurrent neural network* (RNN) is a directed graph consisting of altogether  $N$  nodes, called *neurons*.  $x(t)$  denotes the *activation* of the neuron  $x$  at (discrete) time  $t$ . We may distinguish three groups of neurons (cf. Figure 1):

- *input* neurons (usually without incoming edges) whose activation is given by an external source, e.g., a time series,
- *output* neurons (usually without outgoing edges) whose activation represents some output function, and
- *reservoir* or *hidden* neurons (arbitrarily connected) that are used for auxiliary computations.

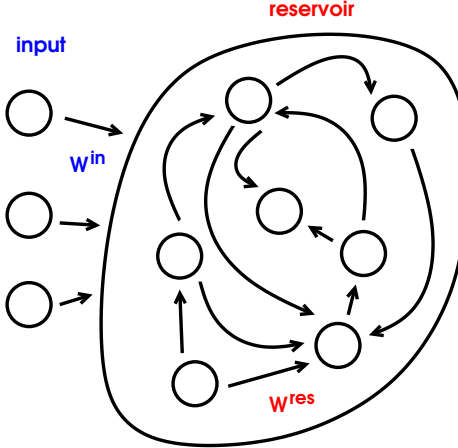


Figure 1: General recurrent neural network. In ESNs, only output weights are trained and the hidden layer is also called reservoir.

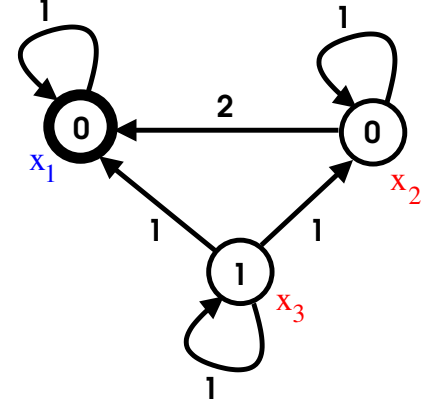


Figure 2: LRNN for  $f(t) = t^2$  with time step  $\tau = 1$ . The input/output neuron  $x_1$  is marked by a thick border. The initial values of the neurons at time  $t_0 = 0$  are written in the nodes. The weights are annotated at the edges.

The edges of the graph represent the network connections. They are usually annotated with *weights* which are compiled in the *transition matrix*  $W$ . An entry  $w_{ij}$  in row  $i$  and column  $j$  denotes the weight of the edge from neuron  $j$  to neuron  $i$ . If there is no connection, then  $w_{ij} = 0$ . The transition matrix has the form

$$W = \begin{bmatrix} W^{\text{out}} \\ W^{\text{in}} \quad W^{\text{res}} \end{bmatrix} \quad (1)$$

containing the following weight matrices:

- *input* weights  $W^{\text{in}}$  (weights from the input and possibly the output to the reservoir),
- *output* weights  $W^{\text{out}}$  (all weights to the output and possibly back to the input), and
- *reservoir* weights  $W^{\text{res}}$  (weights within the reservoir, a matrix of size  $N^{\text{res}} \times N^{\text{res}}$  where  $N^{\text{res}}$  is the number of reservoir neurons).

Let us now define the *network activity*: The initial configuration of the neural network is given by a column vector  $s$  with  $N$  components, called *start vector*. It represents the network state at the start time  $t = t_0$ . Because of the discrete time model, the activation of a (non-input) neuron  $x$  at time  $t + \tau$  (for some time step  $\tau > 0$ ) from the activation at time  $t$  of the neurons  $x_1, \dots, x_n$  that are connected to  $x$  with the weights  $w_1, \dots, w_n$  is computed as follows:

$$x(t + \tau) = g(w_1 x_1(t) + \dots + w_n x_n(t)) \quad (2)$$

This has to be done simultaneously for all neurons of the network. Here  $g$  is a (real-valued) *activation function*. Although we will not make use of it,  $g$  may be different for different

parts of the network. Usually, a nonlinear, bounded, strictly increasing sigmoidal function  $g$  is used, e.g., the logistic function, the hyperbolic tangent ( $\tanh$ ), or the softplus function (Goodfellow et al., 2016, Sect. 3.10). In the following, we employ simply the (linear) identity function and can still approximate arbitrary time-dependent functions (cf. Property 7).

**Definition 3** (linear recurrent neural network). A *linear recurrent network* (LRNN) is an RNN with the following properties:

1. For the start time, it holds that  $t_0 = 0$ , and  $\tau$  is constant, often  $\tau = 1$ .
2. The initial state  $S(0)$  of the given time series constitutes the first  $d$  components of the start vector  $s$ .
3. For all neurons we have *linear activation*, i.e., everywhere  $g$  is the identity.
4. The weights in  $W^{\text{in}}$  and  $W^{\text{res}}$  are taken randomly, independently, and identically distributed from the standard normal distribution, i.e., the Gaussian distribution with mean  $\mu = 0$  and standard deviation  $\sigma = 1$ , whereas the output weights  $W^{\text{out}}$  are learned (cf. Section 4.1).
5. There is no clear distinction between input and output but only one joint group of  $d$  input/output neurons. They may be arbitrarily connected like the reservoir neurons. We thus can imagine the whole network as a big reservoir because the input/output neurons are not particularly special.

LRNNs can run in one of two *modes*: either receiving input or generating (i.e., predicting) output. In output generating mode, Equation 2 is applied to all neurons including the input/output neurons, whereas in input receiving mode the activation of every input/output neuron  $x$  at time  $t$  is always overwritten with the respective input value at time  $t$  given by the time series  $S$ .

### 3.1 Examples

**Example 1.** The function  $f(t) = t^2$  can be realized by an LRNN (in output generating mode) with three neurons (cf. Figure 2). The respective transition matrix  $W$  and start vector  $s$  are:

$$W = \begin{bmatrix} 1 & 2 & 1 \\ 0 & 1 & 1 \\ 0 & 0 & 1 \end{bmatrix} \text{ and } s = \begin{bmatrix} 0 \\ 0 \\ 1 \end{bmatrix}$$

Consequently, starting at  $t = 0$  with time step  $\tau = 1$ , we have:

- $x_3(0) = 1$ ,  $x_3(t+1) = x_3(t)$ , and hence  $x_3(t) = 1$  in general.
- $x_2(0) = 0$ ,  $x_2(t+1) = x_2(t) + x_3(t) = x_2(t) + 1$ , and hence  $x_2(t) = t$ .
- $x_1(0) = 0$ ,  $x_1(t+1) = x_1(t) + 2x_2(t) + x_3(t) = x_1(t) + 2t + 1$ , and hence  $x_1(t) = t^2$  because of the identity  $(t+1)^2 = t^2 + 2t + 1$  (cf. first row of the transition matrix  $W$ ).

Thus, in the neuron  $x_1$ , the function  $f(t)$  is computed. This is the only input/output neuron.

**Remark 1.** LRNNs are well suited to represent differential equations and to solve them numerically. To see this, consider the homogeneous linear differential equation

$$\sum_{k=0}^n c_k x^{(k)}(t) = 0 \quad (3)$$

where  $c_k \in \mathbb{R}$  are constant coefficients,  $x^{(k)}(t)$  is the  $k$ -th derivative of the function  $x$  with respect to time  $t$ , and  $n > 0$ . For a function  $x$  and its derivative  $\dot{x}$ , we have

$$\dot{x}(t) = \lim_{\tau \rightarrow 0} \frac{x(t + \tau) - x(t)}{\tau} \quad \text{and hence} \quad x(t + \tau) \approx x(t) + \tau \dot{x}(t) \quad (4)$$

for small time steps  $\tau$ . If we consider the difference of Equation 3 between the times  $t + \tau$  and  $t$ , we obtain, after dividing by  $\tau$  and applying Equation 4 to  $x^{(k)}(t)$  for  $k \geq 0$ :

$$x^{(n)}(t + \tau) \approx x^{(n)}(t) - \frac{\tau}{c_n} \sum_{k=0}^{n-1} c_k x^{(k+1)}(t)$$

Therefore, we can solve differential equations approximately by LRNNs with start vector  $s$ , which should satisfy Equation 3, and the following transition matrix:

$$W = \begin{bmatrix} 1 & \tau & 0 & \cdots & 0 \\ 0 & 1 & \tau & \ddots & 0 \\ \vdots & \ddots & \ddots & \ddots & 0 \\ 0 & \cdots & 0 & 1 & \tau \\ 0 & -\tau \frac{c_0}{c_n} & \cdots & -\tau \frac{c_{n-2}}{c_n} & 1 - \tau \frac{c_{n-1}}{c_n} \end{bmatrix}$$

**Example 2.** The exponential function  $\exp(t) = e^t$  can be defined by the differential equation  $\dot{x}(t) = x(t)$ , i.e., we have  $c_0 = 1$  and  $c_1 = -1$  in Equation 3. In consequence, according to Remark 1 and because  $\exp(0) = 1$ , the transition matrix  $W$  and start vector  $s$  of the corresponding LRNN are:

$$W = \begin{bmatrix} 1 & \tau \\ 0 & 1 + \tau \end{bmatrix} \quad \text{and} \quad s = \begin{bmatrix} 1 \\ 1 \end{bmatrix}$$

Induction over time yields immediately  $x(t) = \dot{x}(t) = (1 + \tau)^{t/\tau} \approx e^t$  for small  $\tau$  (according to Euler) as expected.

The strong relationship between RNNs and differential equations is already known (Kruse et al., 2016, Sect. 9) as well as the extraction of eigenvalues to describe dynamical systems (Strogatz, 2015, Sect. 5). Nevertheless, as we will show in the rest of this paper, the combination of both provides an effective method for network size reduction (cf. Section 4.3) and therefore seems to be worthwhile to be considered by the machine learning community in more detail.

### 3.2 Network Dynamics

An LRNN runs through network states  $f(t)$  for  $t \geq 0$ . It holds (in output generating mode)

$$f(t) = \begin{cases} s, & t = 0 \\ W \cdot f(t-1), & \text{otherwise} \end{cases}$$

and hence simply  $f(t) = W^t \cdot s$ .

**Property 1.** Let  $W = V \cdot J \cdot V^{-1}$  be the Jordan decomposition of the transition matrix  $W$  where  $J$  is the direct sum, i.e., a block diagonal matrix, of one or more Jordan blocks (Horn and Johnson, 2013, Sect. 3.1)

$$J_m(\lambda) = \begin{bmatrix} \lambda & 1 & 0 & \cdots & 0 \\ 0 & \lambda & 1 & \ddots & \vdots \\ \vdots & \ddots & \ddots & \ddots & 0 \\ \vdots & & \ddots & \lambda & 1 \\ 0 & \cdots & \cdots & 0 & \lambda \end{bmatrix}$$

in general with different sizes  $m \times m$  and different eigenvalues  $\lambda$ . Then we have:

$$f(t) = W^t \cdot s = V \cdot J^t \cdot V^{-1} \cdot s$$

If we decompose  $V$  into matrices  $v$  of size  $N \times m$  and the column vector  $V^{-1} \cdot s$  into a stack of column vectors  $w$  of size  $m$ , corresponding to the Jordan blocks in  $J$ , then  $f(t)$  can be expressed as a sum of vectors  $u = v \cdot J_m(\lambda)^t \cdot w$  where the Jordan block powers are upper triangular Toeplitz matrices, i.e., in which each descending diagonal from left to right is constant, with:

$$(J_m(\lambda)^t)_{ij} = \binom{t}{j-i} \lambda^{t-(j-i)} \quad (\text{Horn and Johnson, 2013, Sect. 3.2.5}) \quad (5)$$

**Remark 2.** Although the parameter  $t$  is discrete, i.e., a nonnegative integer number, the values of  $f(t) = W^t \cdot s$  can also be computed for  $t \in \mathbb{R}$  and are always real. For this, we consider the Jordan block powers from Equation 5:

- The definition of the binomial coefficient  $\binom{t}{k} = \frac{t(t-1)\cdots(t-k+1)}{k(k-1)\cdots 1}$  is applicable for real and even complex  $t$  and nonnegative integer  $k$ . For negative  $k$ , we have  $\binom{t}{k} = 0$ .
- For real matrices  $W$ , there are always complex conjugate eigenvalue pairs  $\lambda$  and  $\bar{\lambda}$  and corresponding complex coefficients  $c$  and  $\bar{c}$  (resulting from the vectors  $u$  in Property 1). With  $c = |c| e^{i\psi}$  and  $\lambda = |\lambda| e^{i\omega}$ , we get  $c \lambda^t + \bar{c} \bar{\lambda}^t = |c| |\lambda|^t \cos(\omega t + \psi)$ , applying Euler's formula. This obviously is defined for all  $t \in \mathbb{R}$  and always yields real-valued  $f(t)$ .
- Negative real eigenvalues, i.e., the case  $\lambda < 0$ , should be treated in a special way, namely by replacing  $\lambda^t$  by  $|\lambda|^t \cos(\pi t)$ . Both terms coincide for integer  $t$ , but only the latter is real-valued for all  $t \in \mathbb{R}$ . The powers of positive real eigenvalues  $\lambda$  are always positive and real and hence need no further consideration.

A Jordan decomposition exists for every square matrix  $W$  (Horn and Johnson, 2013, Theorem 3.1.11). But if  $W$  has  $N$  distinct eigenvectors, there is a simpler decomposition, called *eigendecomposition*. The transition matrix  $W$  is *diagonalizable* in this case, i.e., similar to a diagonal matrix  $D$ , and the network dynamics can be directly described by means of the eigenvalues and eigenvectors of  $W$ :

**Property 2.** Let  $W = V \cdot D \cdot V^{-1}$  be the eigendecomposition of the transition matrix  $W$  with column eigenvectors  $v_1, \dots, v_N$  in  $V$  and eigenvalues  $\lambda_1, \dots, \lambda_N$ , on the diagonal of the diagonal matrix  $D$ , sorted in decreasing order with respect to their absolute values. Like every column vector, we can represent the start vector  $s$  as linear combination of the eigenvectors, namely as  $s = x_1 v_1 + \dots + x_N v_N = V \cdot x$  where  $x = [x_1 \dots x_N]^\top$ . It follows  $x = V^{-1} \cdot s$ . Since  $W$  is a linear mapping and for each eigenvector  $v_k$  with eigenvalue  $\lambda_k$  with  $1 \leq k \leq N$  it holds that  $W \cdot v_k = \lambda_k v_k$ , we have  $W \cdot s = W \cdot (x_1 v_1 + \dots + x_N v_N) = x_1 \lambda_1 v_1 + \dots + x_N \lambda_N v_N$ . Induction over  $t$  yields immediately:

$$f(t) = W^t \cdot s = V \cdot D^t \cdot x = x_1 \lambda_1^t v_1 + \dots + x_N \lambda_N^t v_N \quad (6)$$

### 3.3 Long-Term Behavior

Let us now investigate the long-term behavior of an RNN (run in output generating mode) by understanding it as an (autonomous) *dynamic system* (Colonius and Kliemann, 2014; Strogatz, 2015). We will see (in Property 4) that the network dynamics may be reduced to a very small number of neurons in the long run. They determine the behavior for  $t \rightarrow \infty$ . Nevertheless, for smaller  $t$ , the use of many neurons is important for computing short-term predictions.

**Property 3.** In none of the  $N$  dimensions  $f(t) = W^t \cdot s$  grows faster than a polynomial and only single-exponential in  $t$ .

*Proof.* Let  $f_k(t)$  denote the value of the  $k$ -th dimension of  $f(t)$ ,  $\lambda$  be the eigenvalue of  $W$  with maximal absolute value and  $m$  be the maximal (geometric) multiplicity of the eigenvalues of the transition matrix  $W$ . Then, from Property 1, we can easily deduce

$$|f_k(t)| = O(t^m |\lambda|^t)$$

as asymptotic behavior for large  $t$ . □

**Property 4.** Consider an RNN whose transition matrix  $W$  is completely real-valued, has (according to Property 2) an eigendecomposition  $W = V \cdot D \cdot V^{-1}$  with unit spectral radius (i.e., the largest absolute value of all eigenvalues is 1), and all eigenvalues are distinct, e.g., a pure random reservoir. Then, almost all terms  $x_k \lambda_k^t v_k$  in Equation 6 vanish for large  $t$  because for all eigenvalues  $\lambda_k$  with  $|\lambda_k| < 1$  we have  $\lim_{t \rightarrow \infty} \lambda_k^t = 0$ . Although a general real matrix can have more than two complex eigenvalues which are on the unit disk, for a pure random reservoir as considered here, almost always, i.e., with probability close to 1, only the (largest) eigenvalues  $\lambda_1$  and possibly  $\lambda_2$  have the absolute values 1. In consequence, we have one of the following cases:

1.  $\lambda_1 = +1$ . In this case, the network activity contracts to one point, i.e., to a *singularity*:  

$$\lim_{t \rightarrow \infty} f(t) = x_1 v_1$$

2.  $\lambda_1 = -1$ . For large  $t$  it holds that  $f(t) \approx x_1 (-1)^n v_1$ . This means we have an *oscillation* in this case. The dynamic system alternates between the two points  $\pm x_1 v_1$ .
3.  $\lambda_1$  and  $\lambda_2$  are two (properly) complex eigenvalues with absolute value 1. Since  $W$  is a real-valued matrix, the two eigenvalues as well as the corresponding eigenvectors  $v_1$  and  $v_2$  are complex conjugate with respect to each other. Thus, for large  $t$ , we have an *ellipse* trajectory

$$f(t) \approx x_1 \lambda_1^t v_1 + x_2 \lambda_2^t v_2 = \tilde{V} \cdot \tilde{D}^t \cdot \tilde{x}$$

$$\text{where } \tilde{V} = [v_1 \ v_2], \ \tilde{D} = \begin{bmatrix} \lambda_1 & 0 \\ 0 & \lambda_2 \end{bmatrix}, \text{ and } \tilde{x} = \begin{bmatrix} x_1 \\ x_2 \end{bmatrix}.$$

We consider now the latter case in more detail, converting all complex values into real ones (cf. Section 3.4): In this case, the matrix  $\tilde{V}$  consists of the two complex conjugate eigenvectors  $v = v_1$  and  $\bar{v} = v_2$ . From all linear combinations of both eigenvectors  $\ell(\kappa) = \kappa v + \bar{\kappa} \bar{v}$  for  $\kappa \in \mathbb{C}$  with  $|\kappa| = 1$ , we can determine the vectors with extremal lengths. Since we only have two real-valued dimensions because clearly the activity induced by the real matrix  $W$  remains in the real space, there are two such vectors. Let now  $\kappa = e^{i\varphi} = \cos(\varphi) + i \sin(\varphi)$  (Euler's formula) and  $v_{\Re}$  and  $v_{\Im}$  be the real and imaginary parts of  $v$ , respectively, i.e.,  $v = v_{\Re} + i v_{\Im}$  and  $\bar{v} = v_{\Re} - i v_{\Im}$ . Then, for the square of the vector length, it holds:

$$\begin{aligned} \|\ell(\kappa)\|^2 &= \kappa^2 v^2 + 2\kappa \bar{\kappa} v \cdot \bar{v} + \bar{\kappa}^2 \bar{v}^2 = e^{2i\varphi} v^2 + 2v\bar{v} + e^{-2i\varphi} \bar{v}^2 \\ &= 2(\cos(2\varphi)(v_{\Re}^2 - v_{\Im}^2) + (v_{\Re}^2 + v_{\Im}^2) - \sin(2\varphi)(2v_{\Re} \cdot v_{\Im})) \end{aligned}$$

To find out the angle  $\varphi$  with extremal vector length of  $\ell(\kappa)$ , we have to investigate the derivative of the latter term above with respect to  $\varphi$  and compute its zeros. This yields  $2(-2\sin(2\varphi)(v_{\Re}^2 - v_{\Im}^2) - 2\cos(2\varphi)(2v_{\Re} \cdot v_{\Im})) = 0$  and thus  $\tan(2\varphi) = \frac{-2v_{\Re} \cdot v_{\Im}}{v_{\Re}^2 - v_{\Im}^2}$ . Because of the periodicity of the tangent function there are two main solutions for  $\kappa$  that are orthogonal to each other:  $\kappa_1 = e^{i\varphi}$  and  $\kappa_2 = e^{i(\varphi + \pi/2)}$ . They represent the main axes of an ellipse. All points the dynamic system runs through lie on this ellipse in the long run. The length ratio of the ellipse axes is  $\mu = \|\ell(\kappa_1)\| / \|\ell(\kappa_2)\|$ . We normalize both vectors to unit length and put them in the matrix  $\hat{V} = [\ell(\kappa_1) / \|\ell(\kappa_1)\| \quad \ell(\kappa_2) / \|\ell(\kappa_2)\|]$ .

We now build a matrix  $\hat{D}$ , similar to  $\tilde{D}$  but completely real-valued which states the ellipse rotation. The rotation speed can be derived from the eigenvalue  $\lambda_1$ . In each step of length  $\tau$ , there is a rotation by the angle  $\omega\tau$  where  $\omega$  is the angular frequency which can be determined from the equation  $\lambda_1 = |\lambda_1| e^{i\omega\tau}$ . The two-dimensional ellipse trajectory can be stated by two (co)sinusoids:  $f(t) = [a \cos(\omega t) \ b \sin(\omega t)]^\top$  with  $a, b > 0$ . Applying the addition theorems of trigonometry, we get:

$$\begin{aligned} f(t + \tau) &= \begin{bmatrix} a \cos(\omega(t + \tau)) \\ b \sin(\omega(t + \tau)) \end{bmatrix} \\ &= \begin{bmatrix} a(\cos(\omega t) \cos(\omega\tau) - \sin(\omega t) \sin(\omega\tau)) \\ b(\sin(\omega t) \cos(\omega\tau) + \cos(\omega t) \sin(\omega\tau)) \end{bmatrix} \\ &= \underbrace{\begin{bmatrix} \cos(\omega\tau) & -a/b \sin(\omega\tau) \\ b/a \sin(\omega\tau) & \cos(\omega\tau) \end{bmatrix}}_{\hat{D}} \cdot f(t) \end{aligned}$$

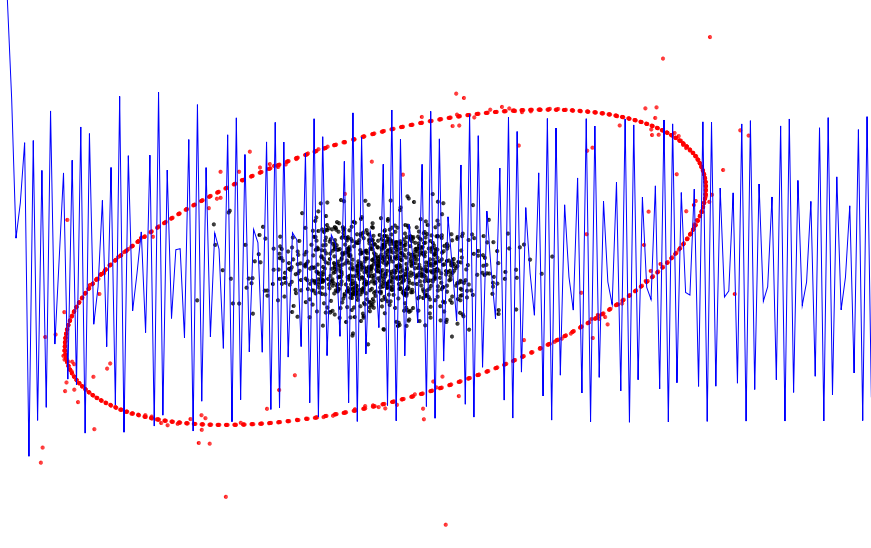


Figure 3: Dynamic system behavior in two dimensions (qualitative illustration): In the long run, we get an ellipse trajectory (dotted/red), though the original data may look like random (dots/black). Projected to one dimension, we have pure sinusoids with one single angular frequency, sampled in large steps (solid/blue).

From this, we can read off the desired ellipse rotation matrix  $\hat{D}$  as indicated above and  $\mu = a/b$ . Finally, we can determine the corresponding two-dimensional start vector  $\hat{x}$  by solving the equation  $\hat{V} \cdot \hat{D} \cdot \hat{x} = \tilde{V} \cdot \tilde{D} \cdot \tilde{x}$ . In summary, we have

$$f(t) \approx \hat{V} \cdot \hat{D}^t \cdot \hat{x} \quad (7)$$

for large  $t$ . Every RNN with many neurons can thus be approximated by a simple network with at most two neurons, defined by the matrix  $\hat{D}$  and start vector  $\hat{x}$ . The output values can be computed for all original dimensions by multiplication with the matrix  $\hat{V}$ . They lie on an ellipse in general. Nonetheless, in the beginning, i.e., for small  $t$ , the dynamics of the system is not that regular (cf. Figure 3). But although Property 4 states the asymptotic behavior of random RNNs with unit spectral radius, interestingly the network dynamics converges relatively fast to the final ellipse trajectory: The (Euclidean) distance between the actual value  $f(t)$  (according to Equation 6) and its approximation by the final ellipse trajectory (Equation 7) is almost zero already after a few hundred steps (cf. Figure 4). Of course this depends on the eigenvalue distribution of the transition matrix (Tao et al., 2010).

The long-term behavior of LRNNs is related to that of ESNs. For the latter, usually the activation function is  $\tanh$  and the spectral radius is smaller than 1. Then reservoirs with zero input collapse because of  $|\tanh(z)| \leq z$  for all  $z \in \mathbb{R}$  but the convergence may be rather slow. This leads to the so-called *echo state property* (Manjunath and Jaeger, 2013): Any random initial state of a reservoir is forgotten such that, after a washout period, the current network state is a function of the driving input. In contrast to ESNs, LRNNs have linear activation and usually a spectral radius of exactly 1. But as we have just shown, there

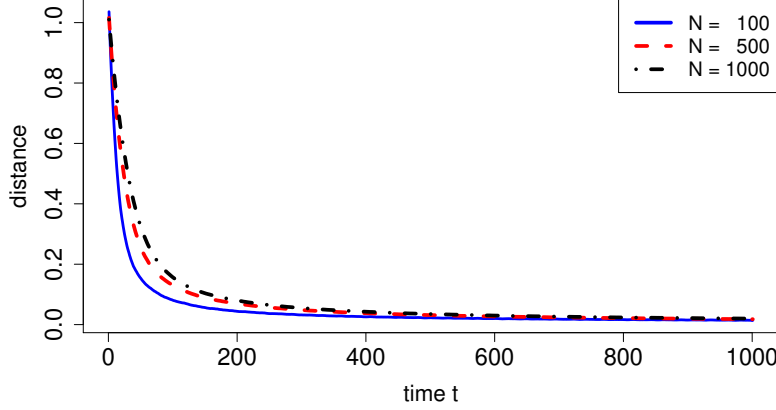


Figure 4: Asymptotic behavior of random reservoirs with unit spectral radius: The (Euclidean) distance between the actual value  $f(t)$  (according to Equation 6) and its approximation by the final ellipse trajectory (Equation 7) is almost zero already after a few hundred steps. The figure shows the distances for  $N = 100$  (solid/blue),  $N = 500$  (dashed/red), and  $N = 1000$  (dotted/black) random reservoir neurons, starting with a random vector of unit length, averaged over 1000 trials.

is a similar effect in the long run: The network activity reduces to at most two dimensions which are independent from the initial state of the network.

### 3.4 Real-Valued Transition Matrix Decomposition

For real-valued transition matrices  $W$ , it is possible to define a decomposition that, in contrast to the ordinary Jordan decomposition in Property 1, solely makes use of real-valued components, adopting the so-called *real Jordan canonical form* (Horn and Johnson, 2013, Sect. 3.4.1) of the square matrix  $W$ . For this completely real-valued decomposition, the Jordan matrix  $J$  is transformed as follows:

1. A Jordan block with real eigenvalue  $\lambda$  remains as is in  $J$ .
2. For complex conjugate eigenvalue pairs  $\lambda = \lambda_{\Re} + i\lambda_{\Im}$  and  $\bar{\lambda} = \lambda_{\Re} - i\lambda_{\Im}$  with  $\lambda_{\Re}, \lambda_{\Im} \in \mathbb{R}$ , the direct sum of the corresponding Jordan blocks  $J_m(\lambda)$  and  $J_m(\bar{\lambda})$  is replaced by a real Jordan block:

$$\begin{bmatrix} M & I & O & \cdots & O \\ O & M & I & \ddots & \vdots \\ \vdots & \ddots & \ddots & \ddots & O \\ \vdots & & \ddots & M & I \\ O & \cdots & \cdots & O & M \end{bmatrix} \text{ with } M = \begin{bmatrix} \lambda_{\Re} & \lambda_{\Im} \\ -\lambda_{\Im} & \lambda_{\Re} \end{bmatrix}, I = \begin{bmatrix} 1 & 0 \\ 0 & 1 \end{bmatrix} \text{ and } O = \begin{bmatrix} 0 & 0 \\ 0 & 0 \end{bmatrix}$$

This procedure yields the real Jordan matrix  $J$ . In consequence, we have to transform  $V$  also into a completely real-valued form. For a complex conjugate eigenvalue pair  $\lambda$  and  $\bar{\lambda}$ , the corresponding two eigenvectors in  $V$  could be replaced by the vectors in  $\hat{V}$  (cf. Section 3.3). The subsequent theorem shows a more general way: The matrix  $V$  from Property 1 is transformed into a real matrix  $A$  and, what is more, the start vector  $s$  can be replaced by an arbitrary column vector  $y$  with all non-zero entries.

**Property 5.** Let  $W = V \cdot J \cdot V^{-1}$  be the (real) Jordan decomposition of the transition matrix  $W$  and  $s$  the corresponding start vector. Then for all column vectors  $y$  of size  $N$  with all non-zero entries, there exists a square matrix  $A$  of size  $N \times N$  such that for all integer  $t \geq 0$  we have:

$$f(t) = W^t \cdot s = A \cdot J^t \cdot y$$

*Proof.* We first prove the case where the Jordan matrix  $J$  only contains ordinary Jordan blocks as in Property 1, i.e., possibly with complex eigenvalues on the diagonal. Since  $J$  is a direct sum of Jordan blocks, it suffices to consider the case where  $J$  is a single Jordan block because, as the Jordan matrix  $J$ , the matrices  $A$  and also  $B$  (see below) can be obtained as direct sums, too.

In the following, we use the column vectors  $y = [y_1 \cdots y_N]^\top$  with all non-zero entries,  $x = [x_1 \cdots x_N]^\top$  with  $x = V^{-1} \cdot s$ , and  $b = [b_1 \cdots b_N]^\top$ . From  $b$ , we construct the following upper triangular Toeplitz matrix

$$B = \begin{bmatrix} b_N & \cdots & b_2 & b_1 \\ 0 & \ddots & & b_2 \\ \vdots & \ddots & \ddots & \vdots \\ 0 & \cdots & 0 & b_N \end{bmatrix}$$

which commutes with the Jordan block  $J$  (Horn and Johnson, 2013, Sect. 3.2.4), i.e., it holds that (a)  $J \cdot B = B \cdot J$ . We define  $B$  and hence  $b$  by the equation (b)  $x = B \cdot y$  which is equivalent to:

$$\begin{bmatrix} y_N & \cdots & y_2 & y_1 \\ 0 & \ddots & & y_2 \\ \vdots & \ddots & \ddots & \vdots \\ 0 & \cdots & 0 & y_N \end{bmatrix} \cdot b = \begin{bmatrix} x_1 \\ x_2 \\ \vdots \\ x_N \end{bmatrix}$$

Since the main diagonal of the left matrix contains no 0s because  $y_N \neq 0$  by precondition, there always exists a solution for  $b$  (Horn and Johnson, 2013, Sect. 0.9.3). Then  $A = V \cdot B$  does the job:

$$f(t) = W^t \cdot s \stackrel{\text{Property 1}}{=} V \cdot J^t \cdot V^{-1} \cdot s = V \cdot J^t \cdot x \stackrel{(b)}{=} V \cdot J^t \cdot B \cdot y \stackrel{(a)}{=} V \cdot B \cdot J^t \cdot y = A \cdot J^t \cdot y$$

The generalization to the real Jordan decomposition is straightforward by applying the fact that for complex conjugate eigenvalue pairs  $\lambda$  and  $\bar{\lambda}$  the matrix  $M$  from above in a real Jordan block is similar to the diagonal matrix  $D = \begin{bmatrix} \lambda & 0 \\ 0 & \bar{\lambda} \end{bmatrix}$  via  $U = \begin{bmatrix} -i & -i \\ 1 & -1 \end{bmatrix}$  (Horn and Johnson, 2013, Sect. 3.4.1), i.e.,  $M = U \cdot D \cdot U^{-1}$ . The above-mentioned commutation property (a) analogously holds for real Jordan blocks. This completes the proof.  $\square$

## 4. Learning LRNNs

Functions can be learned and approximated by LRNNs in two steps: First, as for ESNs (Jaeger and Haas, 2004), we only learn the output weights  $W^{\text{out}}$  (cf. Section 4.1); all other connections remain unchanged. The input weights  $W^{\text{in}}$  and reservoir weights  $W^{\text{res}}$  are arbitrary random values that are not changed (cf. Definition 3). Nevertheless, in order to obtain better numerical stability during the computation, they are adjusted as follows:

- In the presence of linear activation, the spectral radius of the reservoir weights matrix  $W^{\text{res}}$  is set to 1. Otherwise, with increasing  $t$ , the values of  $W^t$  explode if the spectral radius is greater or vanish if the spectral radius is smaller than 1 (cf. Section 3.3).
- The norms of the vectors in  $W^{\text{in}}$  and  $W^{\text{res}}$  should be balanced (Koryakin et al., 2012). To achieve this, we initialize the reservoir neurons such that the reservoir start vector  $r_0$  (with  $N^{\text{res}}$  components) has unit norm by setting:

$$r_0 = \frac{1}{\sqrt{N^{\text{res}}}} \cdot [1 \cdots 1]^{\top}$$

It is part of the start vector  $s = \begin{bmatrix} S(0) \\ r_0 \end{bmatrix}$  (cf. Section 3).

- We usually employ fully connected graphs, i.e., all, especially the reservoir neurons are connected with each other because the connectivity has nearly no influence on the best reachable performance (Koryakin et al., 2012).

Second, if possible, we reduce the network size (cf. Section 4.3); this often leads to better generalization and avoids overfitting. Thus, in contrast to many other approaches, the network architecture is changed during the learning process. In contrast to other approaches, we do not do this by incremental derivation from the original network but in only one step.

### 4.1 Learning the Output Weights

To learn the output weights  $W^{\text{out}}$ , we run the input values from the time series  $S(0), \dots, S(n)$  through the network (in input receiving mode), particularly through the reservoir. This means, we build the sequence of corresponding reservoir states  $R(0), \dots, R(n)$  where the reservoir start vector  $r_0$  in principle can be chosen arbitrarily but with all non-zero entries (cf. Property 5):

$$R(t_0) = r_0 \text{ and } R(t + \tau) = [W^{\text{in}} \ W^{\text{res}}] \cdot \begin{bmatrix} S(t) \\ R(t) \end{bmatrix} \quad (8)$$

We want to predict the next input value  $S(t + \tau)$ , given the current input and reservoir states  $S(t)$  and  $R(t)$ . To achieve this, we comprise all but the last input and reservoir states in one matrix  $X$  with:

$$X = \begin{bmatrix} S(0) & \dots & S(n-1) \\ R(0) & \dots & R(n-1) \end{bmatrix} \quad (9)$$

Each output value corresponds to the respective next input value  $S(t + \tau)$ . Therefore, we compose another matrix

$$Y^{\text{out}} = [S(1) \ \dots \ S(n)] \quad (10)$$

consisting of the predicted next values of the time series  $S$  where the first value  $S(0)$  clearly has to be omitted because it cannot be predicted. We compute  $Y^{\text{out}}(t) = S(t + \tau)$  from  $X(t)$  by assuming a linear dependency:

$$Y^{\text{out}} = W^{\text{out}} \cdot X \quad (11)$$

Its solution can easily be determined as  $W^{\text{out}} = Y^{\text{out}}/X$ , where  $/$  denotes right matrix division, i.e., the operation of solving a linear equation system, possibly applying the least squares method in case of an overdetermined system, as implemented in many scientific programming languages like Matlab (Higham and Higham, 2017) or Octave (Eaton et al., 2017). Prediction of further values is now possible (in output generating mode) as follows:

$$\begin{bmatrix} S(t + \tau) \\ R(t + \tau) \end{bmatrix} = W \cdot \begin{bmatrix} S(t) \\ R(t) \end{bmatrix} \text{ with } W \text{ as in Equation 1} \quad (12)$$

**Property 6** (treatment of multiple sequences). It is also possible to learn from multiple sequences at once. For this, let several time series  $S_1, \dots, S_K$  in  $d$  dimensions with (not necessarily identical) lengths  $n_1, \dots, n_K$  be given. For each  $S_k$  with  $1 \leq k \leq K$ , we determine:

- the sequence of corresponding reservoir states  $R_k$  (according to Equation 8), taking always the same reservoir start vector  $r_0$ ,
- the corresponding input matrix  $X_k$  (according to Equation 9), and
- the corresponding predicted output matrix  $Y_k^{\text{out}}$  (according to Equation 10).

We aggregate the input and output matrices to  $X = [X_1 \dots X_K]$  and  $Y^{\text{out}} = [Y_1^{\text{out}} \dots Y_K^{\text{out}}]$  with  $n_1 + \dots + n_K$  columns each. Solving the linear matrix equation  $Y^{\text{out}} = W^{\text{out}} \cdot X$  (identical with Equation 11) finally yields the output weight matrix  $W^{\text{out}}$ .

This first phase of the learning procedure is related to a linear *autoregressive model* (Akaike, 1969). However, one important difference to an autoregressive model is that for LRNNs the output does not only depend on its own previous values and possibly white noise but on the complete state of the possibly big reservoir whose dynamics is explicitly dealt with in the reservoir matrix  $W^{\text{res}}$ . The reservoir effectively allows us to do arbitrary auxiliary computation such that any (non-linear) function  $f(t)$  can be approximated by an LRNN (cf. Property 7).

## 4.2 An Approximation Theorem

**Property 7.** From a function  $f(t)$  in  $d \geq 1$  dimensions, let a series of function values  $f(t_0), \dots, f(t_n)$  be given. Then there is an LRNN with the following properties:

1. It runs exactly through all given  $n + 1$  function values, i.e., it approximates  $f(t)$ .
2. It can effectively be learned by the above-stated solution procedure (Section 4.1).

*Proof.* The procedure for learning output weights (cf. Section 4.1) uses the reservoir state sequence as part of the coefficient matrix  $X$  which reduces to at most two dimensions in the long run however – independent of the number of reservoir neurons (cf. Section 3.3).

Thus, the rank of the coefficient matrix  $X$  is not maximal in general and in consequence the linear equation system from Equation 11 often has no solutions (although we may have an equation system with the same number of equations and unknowns). A simple increase of the number of reservoir neurons does not help much. Therefore, we shall apply the learning procedure in a specific way, learning not only the output weights  $W^{\text{out}}$  as in ESNs but the complete transition matrix  $W$  as follows:

First, we take the series of function values  $f(t_0), \dots, f(t_n)$  and identify them with the time series  $S(0), \dots, S(n)$ . Let then  $[R(0) \dots R(n)]$  be a random reservoir state sequence matrix for  $N^{\text{res}}$  reservoir neurons, considered as additional input in this context. If all elements of this matrix are random numbers, independently and identically distributed from the standard normal distribution, its rank is almost always maximal. Let now  $d'$  be the rank of the matrix  $[S(0) \dots S(n-1)]$  and:

$$Y = \begin{bmatrix} S(1) & \dots & S(n) \\ R(1) & \dots & R(n) \end{bmatrix}$$

We now have to solve the linear matrix equation  $W \cdot X = Y$  with  $X$  as in Equation 9. If  $w_1, \dots, w_N$  and  $y_1, \dots, y_N$  denote the row vectors of the matrices  $W$  and  $Y$ , respectively, then this is equivalent to simultaneously solving the equations  $w_k \cdot X = y_k$ , for  $1 \leq k \leq N$ . We must ensure that there exists almost always at least one solution. This holds if and only if the rank of the coefficient matrix  $X$  is equal to the rank of the augmented matrix  $M_k = \begin{bmatrix} X \\ y_k \end{bmatrix}$ , for every  $k$ . We obtain the equation  $\text{rank}(X) = \min(d' + N^{\text{res}}, n) = \text{rank}(M_k) = \min(d' + N^{\text{res}} + 1, n)$ . From this, it follows that

$$N^{\text{res}} \geq n - d' \tag{13}$$

reservoir neurons have to be employed to guarantee at least one exact solution for the  $w_k$ . By construction, the neural network with transition matrix  $W$  runs exactly through all given  $n + 1$  function values  $f(t)$ .  $\square$

**Remark 3.** The just sketched proof of Property 7 suggests a way to learn the input and reservoir weights. This topic has also been investigated by Palangi et al. (2013) for ESNs with nonlinear activation function in the reservoir. However, for LRNNs, the given input and reservoir weights  $W^{\text{in}}$  and  $W^{\text{res}}$  together with the learned output weights  $W^{\text{out}}$  already provide the best approximation of the function  $f(t)$ . There is no need to learn the input and reservoir weights, simply because LRNNs are completely linearly activated RNNs (including the reservoir). If one tries to learn  $W^{\text{in}}$  and  $W^{\text{res}}$  taking not only the output time series  $S$  but additionally the reservoir state time series  $R$  into account, then exactly the given input and reservoir weights are learned (if Equation 13 holds). Only with nonlinear activation there is a learning effect. Nonetheless,  $W^{\text{in}}$  and  $W^{\text{res}}$  can be learned by the procedure sketched in the proof, if they are not given in advance, starting with a random reservoir state sequence. But our experiments indicate that this procedure is less numerically stable than the one with given, i.e., predefined input and reservoir weights and unit spectral radius for the reservoir (cf. Section 4.1).

Property 7 is related to the *universal approximation theorem* for feedforward neural networks (Hornik, 1991). It states that a (non-recurrent) network with a linear output layer and

at least one hidden layer activated by a nonlinear, sigmoidal function can approximate any continuous function on a closed and bounded subset of the  $\mathbb{R}^n$  from one finite-dimensional space to another with any desired non-zero amount of error, provided that the network is given enough hidden neurons (Goodfellow et al., 2016, Sect. 6.4.1). Since RNNs are more general than feedforward networks, the universal approximation theorem also holds for them (Maass et al., 2002). Any measurable function can be approximated with a (general) recurrent network arbitrarily well in probability (Hammer, 2000).

Because of the completely linear activation, LRNNs cannot compute a nonlinear function  $f(x)$  from the (possibly multi-dimensional) input  $x$ . Nevertheless, they can approximate any (possibly nonlinear) function over time  $f(t)$ , as Property 7 shows. Another important difference between LRNNs and nonlinearly activated feedforward neural networks is that LRNNs can learn the function  $f(t)$  efficiently. No gradient-descent method like backpropagation is required; we just have to solve a linear equation system. Hence learning is as easy as learning a single-layer perceptron, which however is restricted in expressibility because only linearly separable functions can be represented.

**Remark 4.** Any time series  $S(0), \dots, S(n)$  can be generated by employing a backward shift matrix, i.e., a binary matrix with 1s on the subdiagonal and 0s elsewhere (Horn and Johnson, 2013, Sect. 0.9.7), as transition matrix  $W$  and  $s = [S(0) \cdots S(n)]^\top$  as start vector. But such a network clearly would have no ability to generalize to future data. Fortunately, this does not hold for a transition matrix  $W$  learned by the procedure in Section 4.1. Furthermore, the eigenvalue spectrum of the backward shift matrix is empty, whereas that of the learned  $W$  is not, which is important for network size reduction introduced in Section 4.3.

### 4.3 Network Size Reduction

To approximate a function exactly for sure, we need a large number  $N^{\text{res}}$  of reservoir neurons in Property 7. It is certainly a good idea to lower this number. One could do this by simply taking a smaller number of reservoir neurons, but then a good approximation cannot be guaranteed. In what follows, we therefore reduce the dimensionality of the transition matrix  $W$  in a more controlled way – after learning the output weights. Our procedure of dimensionality reduction leads to smaller networks with sparse connectivity. In contrast to other approaches, we do not learn the new network architecture by incremental derivation from the original network, e.g., by removing unimportant neurons or weights, but in only one step by inspecting the eigenvalues of the transition matrix.

For ESNs, dimensionality reduction is considered, too, namely by means of so-called *conceptors* (Jaeger, 2014, 2017; Krause et al., 2021). These are special matrices which restrict the reservoir dynamics to a linear subspace that is characteristic for a specific pattern. However, as in principal component analysis (PCA) (Jolliffe, 2011), conceptors reduce only the spatial dimensionality of the point cloud of the given data. In contrast to this, for LRNNs, we reduce the transition matrix  $W$  and hence take also into account the temporal order of the data points in the time series. By applying insights from linear algebra, the actual network size can be reduced and not only the subspace of computation as with conceptors.

**Property 8.** By Property 5, the function  $f(t) = W^t \cdot s$  can be rewritten by means of the Jordan matrix of the transition matrix  $W$  as  $A \cdot J^t \cdot y$ , where the start vector can be

chosen as non-zero constant, e.g.,  $y = [1 \cdots 1]^\top$ . Furthermore, by Property 1,  $f(t)$  can be expressed as a sum of vectors  $u = v \cdot J_m(\lambda)^t \cdot w$  where  $w$  is constant because it is part of the start vector  $y$ . Then it follows from Property 4 that for large  $t$  the contribution of a Jordan component vanishes if  $\|v\| \approx 0$  and/or  $|\lambda| \ll 1$ .

In consequence, we can omit all Jordan components causing only small errors, until a given threshold is exceeded. The error  $E$  of a network component corresponding to a Jordan block  $J_m(\lambda)$  can be estimated by the root-mean-square error (RMSE) normalized to the number of all sample components between input  $x$  and predicted output  $y$ :

$$\text{RMSE}(x, y) = \sqrt{\frac{1}{n} \sum_{t=1}^n \|x(t) - y(t)\|^2}$$

In practice, we omit all network components with smallest errors as long as the RMSE is below a given threshold  $\theta$ . Network components that are not omitted are considered *relevant*. Thus, from  $A$ ,  $J$ , and  $y$  (according to Property 5), we successively derive reduced matrices  $A'$  and  $J'$  and the vector  $y'$  as follows:

- From  $A$ , take the rows corresponding to the input/output components and the columns corresponding to the relevant network components.
- From  $J$ , take the rows and columns corresponding to the relevant network components.
- From  $y$ , take the rows corresponding to the relevant network components.

Note that the dimensionality reduction does not only lead to a smaller number of reservoir neurons, but also to a rather simple network structure: The transition matrix  $J'$  (which comprises the reservoir weights  $W^{\text{res}}$  of the reduced network) is a sparse matrix with non-zero elements only on the main and immediately adjacent diagonals. Thus, the number of connections is in  $O(N)$ , i.e., linear in the number of reservoir neurons, not quadratic – as in general.

Figure 5 summarizes the overall learning procedure for LRNNs including network size reduction. It has been implemented by the authors in Octave. Note that, although the Jordan matrix  $J$  (cf. Property 1) may contain eigenvalues with multiplicity greater than 1, Octave does not always calculate exactly identical eigenvalues in this case. Therefore, we cluster the computed eigenvalues as follows: If the distance in the complex plane between eigenvalues is below some given small threshold  $\delta$ , they are put into the same cluster which eventually is identified with its centroid. Thus it is a kind of single linkage clustering (Gower and Ross, 1969). The complete implementation of the learning procedure together with some case studies (cf. Section 5) is available under the following link:

<https://bitbucket.org/oliverobst/decorating>

#### 4.4 Complexity and Generalization of the Procedure

**Property 9.** In both learning steps, it is possible to employ any of the many available fast and constructive algorithms for linear regression and eigendecomposition (Demmel et al., 2007). Therefore, the time complexity is just  $O(N^3)$  for both output weights learning and

```

%  $d$ -dimensional function, given sampled, as time series
S = [f(0) ... f(n)]

% random initialization of reservoir and input weights
Win = randn(N, d)
Wres = randn(Nres, Nres)

% learn output weights by linear regression
X = [Wt · s]t=0, ..., n
Yout = [S(1) ... S(n)]
Wout = Yout / X

% transition matrix and its decomposition
W = [Wout
      Win   Wres]
J = jordan_matrix(W)

% network size reduction
y = [1 ... 1]T
Y = [Jt · y]t=0, ..., n
A = X / Y with rows restricted to input/output dimensions
reduce(A, J, y) to relevant components
such that RMSE(S, Out) <  $\theta$ 

```

Figure 5: Pseudocode for learning LRNNs including network size reduction. In the last statement, actually a binary search algorithm is employed for determining the relevant network components with smallest errors. For this, the network components are sorted by their error  $E$ .

dimensionality reduction. In theory, if we assume that the basic numerical operations like  $+$  and  $\cdot$  can be done in constant time, the asymptotic complexity is even a bit better. In practice, however, the complexity depends on the bit length of numbers in floating point arithmetic, of course, and may be worse hence. The size of the learned network is in  $O(N)$  (cf. Section 4.3).

Note that, in contrast, feedforward networks with three threshold neurons already are NP-hard to train (Blum and Rivest, 1992). This results from the fact that the universal approximation theorem for feedforward networks differs from Property 7 because the former holds for multi-dimensional functions and not only time-dependent input. In this light, the computational complexity of  $O(N^3)$  for LRNNs does not look overly expensive. It dominates the overall time complexity of the whole learning procedure because it is not embedded in a time-consuming iterative learning procedure (like backpropagation) as in other state-of-the-art methods.

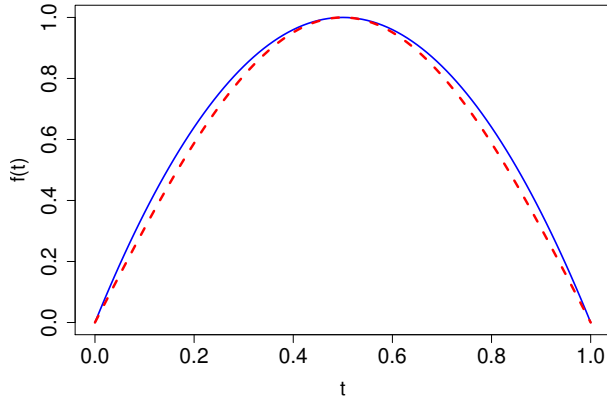


Figure 6: Graphs for Example 3: a parabola and a sinusoid. The question is: which one is which? Both can be learned and distinguished by LRNNs from the visually similar positive parts of the respective graphs, i.e., function values for  $t \in [0, 1]$ . In this interval, all values of the parabola (solid/blue) are greater than or equal to those of the sinusoid (dashed/red).

**Remark 5.** We observe that most of the results presented in this paper still hold if the transition matrix  $W$  contains complex numbers. This means in particular that also complex functions can be learned (from complex-valued time series) and represented by LRNNs (Property 7). Nonetheless, the long-term behavior of networks with a random complex transition matrix  $W$  differs from the one described in Section 3.3 because then there are no longer pairs of complex conjugate eigenvalues.

## 5. Experiments

In this section, we demonstrate evaluation results for learning and predicting time series, approximating them by a function  $f(t)$  represented by an LRNN, for several tasks. We consider the following benchmarks: multiple superimposed oscillators, number puzzles, robot soccer simulation, and predicting stock prices. All experiments are performed with a program written by the authors in Octave (Eaton et al., 2017) (cf. Section 4.3). Let us start with an example that illustrates the overall method.

**Example 3.** The graphs of the functions  $f_1(t) = 4t(1-t)$  (parabola) and  $f_2(t) = \sin(\pi t)$  (sinusoid) look rather similar for  $t \in [0, 1]$  (cf. Figure 6). Can both functions be learned and distinguished from each other by our LRNN learning procedure (cf. Section 4)?

To investigate this, we sample both graphs for  $t \in [0, 1]$  with time step  $\tau = 0.01$ . After that, we learn the output weights  $W^{\text{out}}$  (cf. Section 4.1), starting with a large enough reservoir consisting of up to  $N^{\text{res}} = 100$  neurons (cf. Property 7). Finally, we reduce the size of the overall transition matrix  $W$  with precision threshold  $\theta = 0.01$  and cluster threshold  $\delta = 0.03$  (cf. Section 4.3). Minimal LRNNs consist of  $N_1 = 3$  neurons for the parabola (cf.

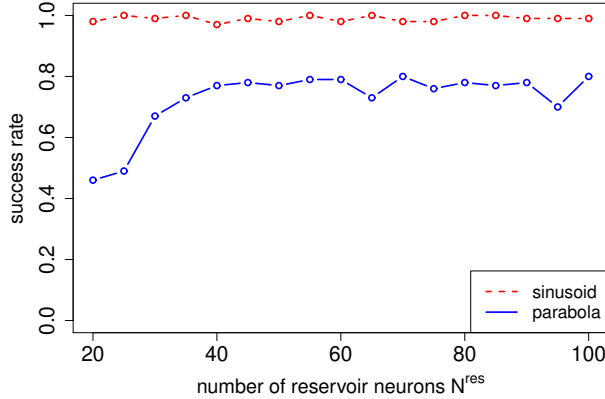


Figure 7: For Example 3, how often LRNNs of minimal size are learned after network size reduction, i.e., with  $N_1 = 3$  neurons for the parabola and  $N_2 = 2$  neurons for the sinusoid? The diagram shows the success rate of the learning procedure in this regard as a function of the number of reservoir neurons  $N^{\text{res}}$  before network size reduction (for 100 trials). Networks of minimal size are learned starting already with  $N^{\text{res}} = 40$  reservoir neurons in about 77% (parabola, solid/blue) or 99% (sinusoid, dashed/red) of the trials.

Example 1) and  $N_2 = 2$  neurons for the sinusoid (cf. Section 3.3). The networks of minimal size are learned already with  $N^{\text{res}} = 40$  reservoir neurons before network size reduction in about 77% (parabola) or 99% (sinusoid) of the trials (cf. Figure 7). Learning the parabola is more difficult because the corresponding transition matrix  $W$  (cf. Example 1) has no proper eigendecomposition according to Property 2 but only a Jordan decomposition according to Property 1.

### 5.1 Multiple Superimposed Oscillators

**Example 4.** Multiple superimposed oscillators (MSO) count as difficult benchmark problems for RNNs (Koryakin et al., 2012; Schmidhuber et al., 2007). The corresponding time series is generated by summing up several (pure) sinusoids. Formally it is described by

$$S(t) = \sum_{k=1}^K \sin(\alpha_k t)$$

where  $K \leq 8$  denotes the number of sinusoids and  $\alpha_k \in \{0.2, 0.311, 0.42, 0.51, 0.63, 0.74, 0.85, 0.97\}$  their frequencies.

Various publications have investigated the MSO problem with different numbers of sinusoids. We concentrate here solely on the most complex case  $K = 8$  whose graph is shown in Figure 8 because in contrast to other approaches it is still easy to learn for LRNNs. Applying the LRNN learning procedure with precision threshold  $\theta = 0.5$ , we arrive at LRNNs with

only  $N = 16$  reservoir neurons and an RMSE less than  $10^{-5}$ , if we start with a large enough reservoir (cf. Figure 9). Since two neurons are required for each frequency (cf. Section 3.3),  $2K = 16$  is the minimal size. Thus LRNNs outperform the previous state-of-the-art for the MSO task with a minimal number of units. Koryakin et al. (2012) report  $N^{\text{res}} = 68$  as the optimal reservoir size for ESNs, but in contrast to our approach, this number is not further reduced. In general, an LRNN with  $2K$  neurons suffices to represent a signal, which might be a musical harmony (Stolzenburg, 2017), consisting of  $K$  sinusoids. It can be learned by the LRNN learning procedure with dimension reduction.

## 5.2 Solving Number Puzzles

**Example 5.** Number series tests are a popular task in intelligence tests. The function represented by a number series can often be learned also by artificial neural networks, in particular RNNs. Glüge and Wendemuth (2013) list 20 number puzzles (cf. Ragni and Klein, 2011). Among them are the series:

$$\begin{aligned} S_8 &= [28, 33, 31, 36, 34, 39, 37, 42] & f(t) &= f(t-2) + 3 \\ S_9 &= [3, 6, 12, 24, 48, 96, 192, 384] & f(t) &= 2f(t-1) \\ S_{15} &= [6, 9, 18, 21, 42, 45, 90, 93] & f(t) &= 2f(t-2) + 4.5 + 1.5(-1)^{t-1} \\ S_{19} &= [8, 12, 16, 20, 24, 28, 32, 36] & f(t) &= f(t-1) + 4 \end{aligned}$$

We apply the LRNN learning procedure to all 20 number puzzles taking small reservoirs because the number series are short. As a side effect, this leads to learning more general functions, which seems to be fully adequate because number puzzles are usually presented to humans. The first 7 of 8 elements of each series are given as input. In each trial, we repeatedly generate LRNNs, until the RMSE is smaller than  $\theta = 0.1$ . Then the last (8-th) element of the respective series is predicted (according to Equation 12) and rounded to the nearest integer because all considered number series are integer.

Table 1 lists the percentages of correct predictions of the last element for different settings. Here the series with definitions recurring to  $f(t-2)$  but not  $f(t-1)$ , e.g.,  $S_8$  and  $S_{15}$ , turned out to be the most difficult. If we now just add the previous values of the time series, i.e.,  $f(t-2)$ , as clue to the input, then the correctness of the procedure increases significantly: For 19 of 20 number puzzles, the most frequently predicted last element (simple majority) is the correct one. It is predicted in 76.5% on average over all trials and number puzzles. Let us remark that the whole evaluation with altogether  $20 \cdot 50 \cdot 1000 = 1\,000\,000$  trials including possibly repeated network generation and network size reduction ran in only a few minutes on standard hardware.

## 5.3 Replaying Soccer Games

RoboCup (Kitano et al., 1997) is an international scientific robot competition in which teams of multiple robots compete against each other. Its different leagues provide many sources of robotics data that can be used for further analysis and application of machine learning. A *soccer simulation* game lasts 10 mins and is divided into 6000 time steps where the length of each cycle is 100 ms. Logfiles contain information about the game, in particular about the current positions of all players and the ball including velocity and orientation for each cycle.

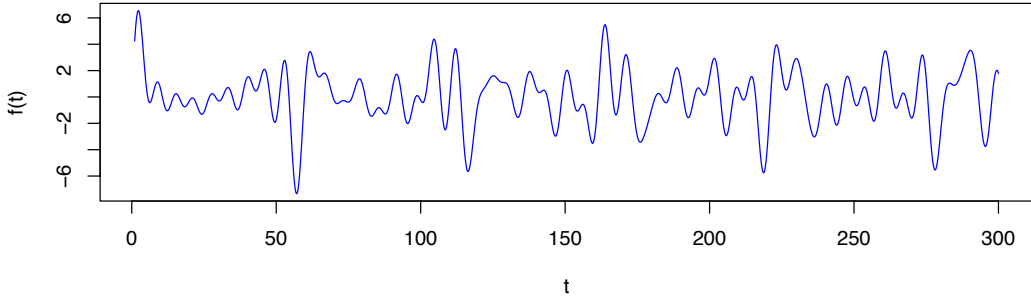


Figure 8: The signal  $S(t)$  of  $K = 8$  multiple superimposed oscillators (for  $1 \leq t \leq 300$  and time step  $\tau = 1$ ) does not have a simple periodic structure. LRNN learning leads to minimal networks with only  $N = 16 = 2K$  reservoir neurons, i.e., two for each frequency in the signal.

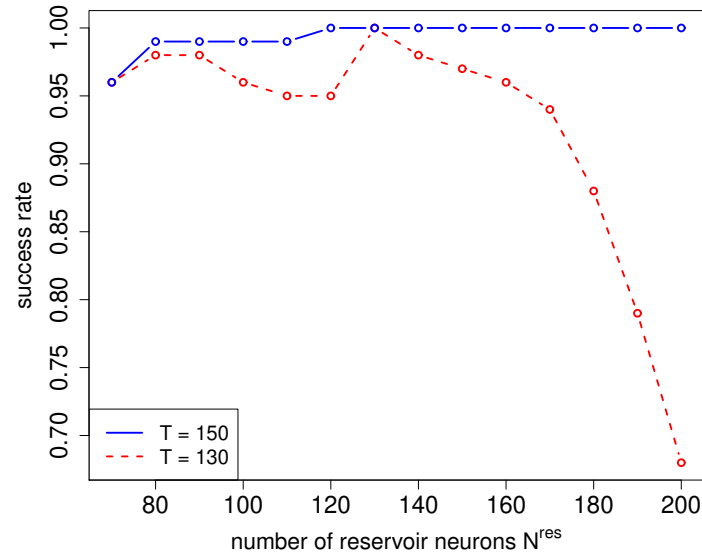


Figure 9: Experimental results for the MSO example ( $K = 8$ ). The diagram shows the success rate (from 100 trials): from an initial reservoir size of  $N^{\text{res}}$  neurons, how often is the minimal LRNN with size  $N = 16$  learned? The two curves are for different lengths  $T$  of the time series  $S(t)$  used for training. Already for  $T = 150$  (solid/blue), a minimal-size LRNN is learned in at least 96% of the trials if  $N^{\text{res}} \geq 70$ . For these minimal LRNNs, the RMSE is smaller than  $10^{-5}$ . As one can see, for  $T = 130$  (dashed/red) the given information does not always suffice and leads to overfitting.

series	$N^{\text{res}} = 3$	$N^{\text{res}} = 4$	$N^{\text{res}} = 5$	with reduction	plus clue
$S_1$	2.2%	1.3%	1.3%	0.8%	33.4%
$S_2$	37.6%	42.2%	29.4%	32.0%	100.0%
$S_3$	5.4%	4.1%	1.1%	3.2%	100.0%
$S_4$	23.8%	24.2%	16.8%	23.2%	99.9%
$S_5$	56.9%	57.6%	44.2%	44.7%	99.7%
$S_6$	31.7%	33.7%	16.1%	11.0%	100.0%
$S_7$	72.8%	68.2%	56.2%	64.5%	100.0%
$S_8$	5.1%	3.4%	1.3%	1.8%	76.3%
$S_9$	100.0%	100.0%	100.0%	100.0%	100.0%
$S_{10}$	48.9%	71.5%	67.6%	72.6%	100.0%
$S_{11}$	10.6%	9.0%	3.4%	3.7%	100.0%
$S_{12}$	23.8%	21.1%	11.0%	8.5%	43.2%
$S_{13}$	56.5%	58.1%	41.5%	47.2%	99.8%
$S_{14}$	6.7%	7.4%	2.1%	2.7%	87.1%
$S_{15}$	1.6%	2.6%	2.5%	0.3%	1.1%
$S_{16}$	6.8%	5.9%	3.4%	2.9%	73.3%
$S_{17}$	11.9%	12.0%	6.8%	6.6%	41.0%
$S_{18}$	3.1%	2.0%	1.1%	0.9%	18.0%
$S_{19}$	59.6%	70.1%	72.0%	77.8%	99.8%
$S_{20}$	1.5%	0.5%	0.6%	0.5%	57.2%

Table 1: Percentages of correct predictions of the last element for 20 number puzzles (Ragni and Klein, 2011; Glüge and Wendemuth, 2013) in 1000 trials for different settings: (a) with fixed reservoir size  $N^{\text{res}} = 3, 4, 5$ ; (b) with network size reduction starting with  $N^{\text{res}} = 7$  reservoir neurons; (c) same procedure but in addition always the previous series value is used as clue.

Michael et al. (2019) describe a research dataset using some of the released binaries of the RoboCup 2D soccer simulation league (Chen et al., 2003; Gabel et al., 2017) from 2016 and 2017 (Michael et al., 2018). In our experiments we evaluated ten games of the top-five teams (available from <https://bitbucket.org/oliverobst/robocupsimdata>), considering only the  $(x, y)$ -coordinates of the ball and the altogether 22 players for all time points during the so-called “play-on” mode.

For LRNN learning, we use only every 10-th time step of each game with  $d = 2 + 2 \cdot 22 = 46$  input dimensions and start with a reservoir consisting of  $N^{\text{res}} = 500$  neurons. We repeat the learning procedure until the RMSE is smaller than 1; on average, already two attempts suffice for this. This means, if we replay the game by the learned LRNN (in output generating mode) then on average the predicted positions deviate less than 1 m from the real ones (Euclidean distance) – over the whole length of the game (cf. Figure 10). Network size reduction leads to significantly less neurons compared to the original number  $N = 46 + 500 = 546$  – on average 29.2% if we concentrate on the relevant components for the ball trajectory (cf. Table 2). Note that the size of the learned network is in  $O(N)$

game	RMSE (1)	RMSE (2)	net size	reduction
#1	0.000 00	0.785 81	385	29.5%
#2	0.000 01	0.969 11	403	26.2%
#3	0.000 04	0.976 80	390	28.6%
#4	0.000 00	0.976 96	406	25.6%
#5	0.000 00	0.984 25	437	20.0%
#6	0.000 00	0.479 39	354	35.2%
#7	0.000 00	0.787 31	390	28.6%
#8	0.002 55	0.987 87	385	29.5%
#9	0.000 00	0.885 18	342	37.4%
#10	0.000 00	0.960 43	376	31.1%

Table 2: For ten RoboCup simulation games, an LRNN is learned with initially  $N = 500 + 46 = 546$  neurons. The table shows the RMSE (1) before and (2) after dimensionality reduction where  $\theta = 1$  m. The network size can be reduced significantly – 29.2% on average (last column).

(cf. Property 9). Thus the LRNN model is definitely smaller than the original time series representation of a game. The complete learning procedure runs in less than a minute on standard hardware.

Property 6 shows how we can learn from multiple time series at once. This is also helpful here because by this procedure we can investigate the overall behavior of a specific robot soccer agent. As example for this, we consider the trajectories of the goalkeeper of the RoboCup simulation team FRA-UNITed during the seeding and the qualifying round of RoboCup Japan Open 2020 (see <http://bit.ly/japanopen2020ssim>). For learning one LRNN from this, we employ a reservoir with  $N^{\text{res}} = 1000$  neurons, adopt again a maximum threshold for the RMSE of  $\theta = 1$  m, and only use every 20-th step of each of the 7 games. The overall trajectory of the FRA-UNITed goalkeeper can be learned easily then (cf. Figure 11). From this, one may conclude that the goalkeeper takes up three basic positions in front of the goal, does not approach the centre line more than about 30 m and hardly leaves the centre line.

#### 5.4 Predicting Stock Prices

Stock price prediction is a topic that receives a considerable amount of attention in finance. Complexity of markets resulting in multiple and sudden changes in trends of stock prices make their prediction a challenge. Consequently, a number of different approaches and methods have been developed, with the autoregressive integrated moving average (ARIMA) model (cf. Section 2.3) being a popular choice. Here we analyze 30 different stocks using the closing stock prices 2016–2019 from <https://de.finance.yahoo.com/> and compare their ARIMA prediction with LRNNs (cf. Litz, 2020).

A standard ARIMA( $p, d, q$ ) model consists of autoregression AR( $p$ ) and a moving average MA( $q$ ). The parameter  $p$  describes the history length (lag order) used to predict the

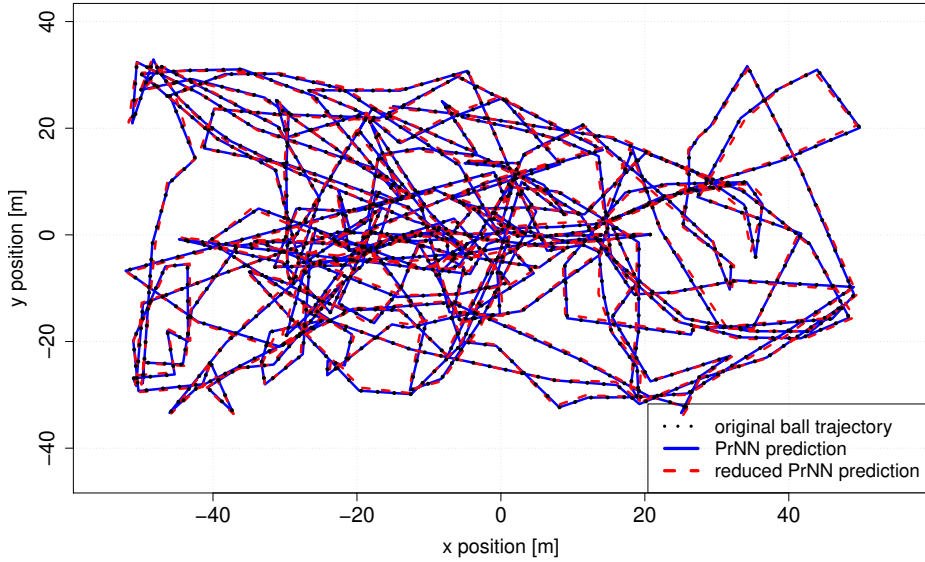


Figure 10: Ball trajectory of RoboCup 2D soccer simulation game #6 (*Oxsy 0* versus *Gliders* 2016) on a pitch of size  $105\text{ m} \times 68\text{ m}$ . For all time steps, the original trajectory of the ball during play is shown (dotted/black). The game can be replayed by an LRNN with  $N = 500 + 46 = 546$  neurons with high accuracy (solid/blue). The reduced network with  $N = 354$  reservoir neurons still mimics the trajectory with only small error (dashed/red).

stock price at time  $t$ . We have  $f(t) = c_1 f(t-1) + \dots + c_p f(t-p) + e_t$  where  $c_1, \dots, c_p$  are (real-valued) autocorrelation coefficients and  $e_t$ , the residuals, are Gaussian white noise. In the moving average process  $\text{MA}(q)$ , the value  $q$  specifies the number of past residuals considered for prediction. An underlying trend of the stock is modeled by using a drift, i.e., a constant that extends the term. This procedure is particularly well-suited for stationary time series. Most financial time series, however, exhibit non-stationary behavior and thus require a transformation to make them stationary. This is achieved by investigating the derivatives of the series, with the order of this process given by the parameter  $d$ .

In our case, we predict each stock using an ARIMA model, implemented with the `auto.arima` package from Hyndman and Khandakar (2008), with seasonal patterns modeled using Fourier terms (Hyndman and Athanasopoulos, 2013, p. 321). To fit the model, we split stock prices into training and test sets, with the first 80% of each series for training and the final 20% used for evaluation. Figure 12 shows predictions of the ARIMA model for Airbus (AIR.DE). We use the first 610 points from this series to build an ARIMA(2,1,2) model with drift and the subsequent 152 data points to evaluate our prediction using the RMSE as metric. Figure 13 shows the prediction using an LRNN for the same task. In this example, the RMSE for LRNNs is  $E_{\text{test}} = 8.07$  Euro and better than the RMSE of the ARIMA model with  $E_{\text{test}} = 9.05$  Euro.

For a representative comparison, we calculate the RMSE of predictions on every stock in the set. The average RMSE using LRNNs is  $E_{\text{test}} = 18.40$  Euro, lower than the average

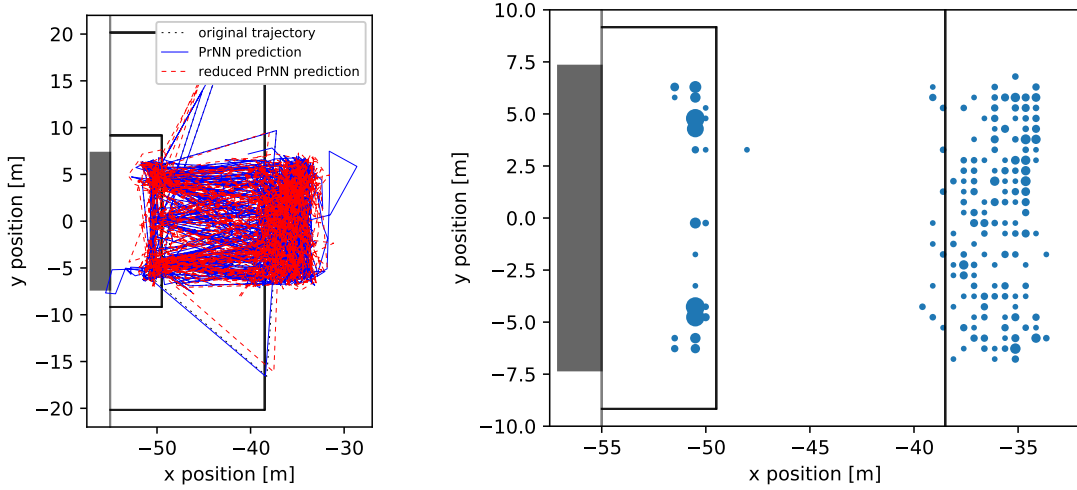


Figure 11: Left: Trajectory of the FRA-UNITed goalkeeper in front of the goal during games at the RoboCup Japan Open 2020. Right: Dots (in blue) mark positions that were visited more than three times (larger dots: more visits, 0.5 m resolution), information that can be derived from predictions, highlighting three larger, frequently visited regions in front of the goal.

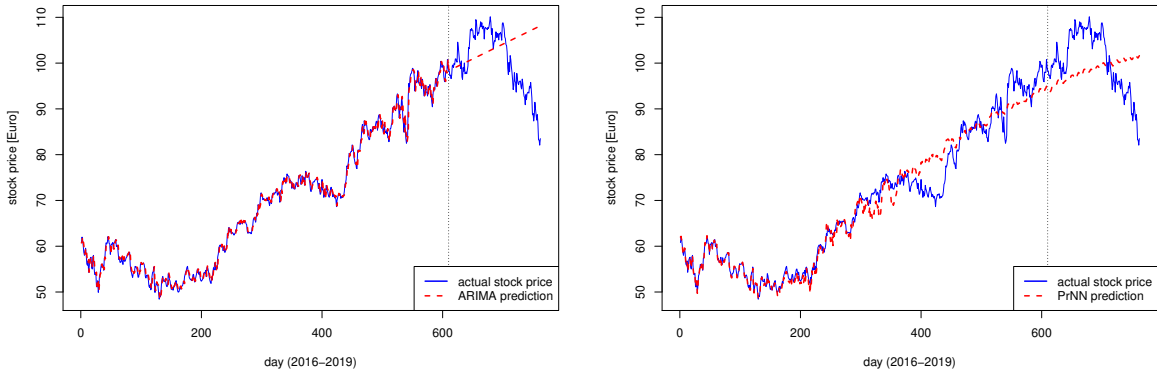


Figure 12: Example stock price (solid/blue) prediction for AIR.DE (Airbus), using an ARIMA(2,1,2) model with drift over the first 610 data points predicting the subsequent 152 data points (dashed/red).

Figure 13: Stock price (solid/blue) prediction for AIR.DE (Airbus) with LRNNs and  $N = 600$  neurons (dashed/red). While residuals during training (the first 610 steps) appear larger than for the ARIMA model, the error on the test set is smaller for LRNNs.

RMSE using ARIMA models with  $E_{\text{test}} = 24.23$  Euro. For shorter term predictions of 60 steps, we were able to slightly reduce the RMSE further to  $E_{\text{test}} = 17.46$  Euro, by using smaller LRNNs of 200 neurons with a smaller training set of 240 points (Litz, 2020). With an average stock price of 286.71 Euro of all stocks in the set, the average deviation is only 6.1%.

Apart from the good prediction results, LRNNs have the advantage that they allow the prediction of multiple stocks at the same time. An LRNN can read in 30 stocks and predict each of them concurrently. For a concurrent forecast for 60 steps, LRNNs using 600 neurons achieved an average RMSE of  $E_{\text{test}} = 30.02$  Euro with 240 training steps. Compared to ARIMA, LRNNs have also an advantage when it comes to the number of hyper-parameters that have to be tuned. The LRNN model is robust when it comes to choosing the number of neurons, whereas the ARIMA model requires the adjustment of many parameters (e.g., for seasonal patterns). With an increase in number of hyper-parameters the compute time for ARIMA also increases. In our example, LRNNs are computed about 15 times faster than the ARIMA models with the selected number of Fourier terms.

The review by Shah et al. (2019) shows that predicting stock prices remains a challenging problem, especially for a longer timeframe, which we have investigated here. Contemporary research often uses complex models, ranging from LSTM RNNs (Nelson et al., 2017; Roondiwala et al., 2017) to attention-based models that use further information about the events that drive the stock prices, e.g., news texts from social media (Liu et al., 2019). These models and also LRNNs yield accurate results, but mainly only in the short run.

## 6. Conclusions

In this paper, we have introduced LRNNs. The major innovation in this work is a closed-form approach to network size reduction (cf. Section 4.3) that learns both architecture and parameters of linearly activated RNNs. No backpropagation, gradient-descent, or other iterative procedure with several epochs is required, and the approach leads to significantly smaller, sparsely connected, and in many cases even minimal size networks.

We have shown that despite its simplicity of using only linear activation in the recurrent layer, LRNNs are a powerful approach to model time-dependent functions. The training procedure only uses standard matrix operations and is thus quite fast. In contrast to ESNs, also, no washout period is required. Any function can be approximated directly from its first step, with an arbitrary starting vector (cf. Property 5).

Although any time-dependent function can be approximated with arbitrary precision (cf. Property 7), not any function can be implemented by RNNs, in particular functions increasing faster than single-exponential (cf. Property 3) like  $2^{2^t}$  (double-exponential) or  $t!$  (factorial function). Nevertheless, experiments with reasonably large example and network sizes can be performed successfully within seconds on standard hardware. However, if thousands of reservoir neurons are employed, the procedure may become numerically unstable, at least our Octave implementation. The likelihood of almost identical eigenvectors and eigenvalues with absolute values greater than 1 in the learned transition matrix  $W$  is increased then. Nonetheless, the underlying major problem here seems to be that existing scientific programming libraries do not calculate the eigenvalues of large matrices accurately enough.

A particularly interesting application of our approach reducing the network size is in hardware implementations of neural networks, e.g., for neuromorphic or reservoir computing (Mead, 1990; Indiveri et al., 2011; Liao and Li, 2017). Neuromorphic computing refers to new hardware that mimics the functioning of the human brain, and neuromorphic hardware results from the exploration of unconventional physical substrates and nonlinear phenomena. Future work shall include improving predictive and memory capacity of LRNNs – analyzed for small networks by Marzen (2017) and to some extent also by Couillet et al. (2016) – taking inspiration from convolutional networks (Goodfellow et al., 2016). Last but not least, other machine learning tasks besides prediction shall be addressed in more detail, including classification and reinforcement learning (Sutton and Barto, 2018; Pong et al., 2017).

## Acknowledgments

We would like to thank Chad Clark, Andrew Francis, Rouven Neitzel, Oliver Otto, Kai Steckhan, Flora Stolzenburg, and Ruben Zilibowitz for helpful discussions and comments. The research reported in this paper has been supported by the German Academic Exchange Service (DAAD) by funds of the German Federal Ministry of Education and Research (BMBF) in the Programmes for Project-Related Personal Exchange (PPP) under grant no. 57319564 and Universities Australia (UA) in the Australia-Germany Joint Research Cooperation Scheme within the project *Deep Conceptors for Temporal Data Mining* (Decorating). A short and preliminary version of this paper was presented at the conference *Cognitive Computing* in Hannover (Stolzenburg et al., 2018). It received the prize for the most technologically feasible poster contribution.

## References

H. Akaike. Fitting autoregressive models for prediction. *Annals of the Institute of Statistical Mathematics*, 21(1):243–247, 1969. URL <http://link.springer.com/content/pdf/10.1007/BF02532251.pdf>.

Y. Bengio, P. Simard, and P. Frasconi. Learning long-term dependencies with gradient descent is difficult. *IEEE Transactions on Neural Networks*, 5(2):157–166, 1994. ISSN 1045-9227. URL <http://doi.org/10.1109/72.279181>.

A. L. Blum and R. L. Rivest. Training a 3-node neural network is NP-complete. *Neural Networks*, 5(1):117–127, 1992. URL [http://doi.org/10.1016/S0893-6080\(05\)80010-3](http://doi.org/10.1016/S0893-6080(05)80010-3).

T. Brown, B. Mann, N. Ryder, M. Subbiah, et al. Language models are few-shot learners. In H. Larochelle, M. Ranzato, R. Hadsell, M. F. Balcan, and H. Lin, editors, *Advances in Neural Information Processing Systems 33 (NeurIPS 2020)*, pages 1877–1901, 2020. URL <http://proceedings.neurips.cc/paper/2020/file/1457c0d6bfc4967418bfb8ac142f64a-Paper.pdf>.

A. Carta, A. Sperduti, and D. Bacciu. Encoding-based memory for recurrent neural networks. *Neurocomputing*, 456:407–420, 2021. ISSN 0925-2312. URL <http://doi.org/10.1016/j.neucom.2021.04.051>.

M. Chen, K. Dorer, E. Foroughi, F. Heintz, Z. Huang, S. Kapetanakis, K. Kostiadis, J. Kummeneje, J. Murray, I. Noda, O. Obst, P. Riley, T. Steffens, Y. Wang, and X. Yin. *Users Manual: RoboCup Soccer Server – for Soccer Server Version 7.07 and Later*. The RoboCup Federation, February 2003. URL [http://helios.hampshire.edu/jdavila/cs278/virtual\\_worlds/robocup\\_manual-20030211.pdf](http://helios.hampshire.edu/jdavila/cs278/virtual_worlds/robocup_manual-20030211.pdf).

F. Colonius and W. Kliemann. *Dynamical Systems and Linear Algebra*, volume 158 of *Graduate Studies in Mathematics*. American Mathematical Society, Providence, Rhode Island, 2014. URL <http://doi.org/10.1090/gsm/158>.

R. Couillet, G. Wainrib, H. Sevi, and H. T. Ali. The asymptotic performance of linear echo state neural networks. *Journal of Machine Learning Research*, 17(178):1–35, 2016. URL <http://jmlr.org/papers/v17/16-076.html>.

J. Demmel, I. Dumitriu, and O. Holtz. Fast linear algebra is stable. *Numerische Mathematik*, 108(1):59–91, 2007. ISSN 0945-3245. URL <http://doi.org/10.1007/s00211-007-0114-x>.

L. Deng and D. Yu. Deep learning: Methods and applications. *Foundations and Trends in Signal Processing*, 7(3-4):198–387, 2014. URL <http://research.microsoft.com/pubs/209355/DeepLearning-NowPublishing-Vol17-SIG-039.pdf>.

J. W. Eaton, D. Bateman, S. Hauberg, and R. Wehbring. *GNU Octave – A High-Level Interactive Language for Numerical Computations*, 2017. URL <http://www.octave.org/>. Edition 4 for Octave version 4.2.1.

J. L. Elman. Finding structure in time. *Cognitive Science*, 14:179–211, 1990. ISSN 0364-0213. URL [http://onlinelibrary.wiley.com/doi/10.1207/s15516709cog1402\\_1](http://onlinelibrary.wiley.com/doi/10.1207/s15516709cog1402_1).

T. Gabel, E. Falkenberg, and E. Godehardt. Progress in RoboCup revisited: The state of soccer simulation 2D. In S. Behnke, R. Sheh, S. Sariel, and D. D. Lee, editors, *RoboCup 2016: Robot Soccer World Cup XX. RoboCup International Symposium*, volume 9776 of *Lecture Notes in Computer Science*, pages 144–156, Leipzig, 2017. Springer Nature Switzerland. URL [http://doi.org/10.1007/978-3-319-68792-6\\_12](http://doi.org/10.1007/978-3-319-68792-6_12).

S. Glüge and A. Wendemuth. Solving number series with simple recurrent networks. In J. M. Ferrández de Vicente, J. R. Álvarez Sánchez, F. de la Paz López, and F. J. Toledo-Moreo, editors, *Natural and Artificial Models in Computation and Biology – 5th International Work-Conference on the Interplay Between Natural and Artificial Computation, IWINAC 2013. Proceedings, Part I*, LNCS 7930, pages 412–420. Springer, 2013. URL [http://doi.org/10.1007/978-3-642-38637-4\\_43](http://doi.org/10.1007/978-3-642-38637-4_43).

I. Goodfellow, Y. Bengio, and A. Courville. *Deep Learning*. Adaptive Computation and Machine Learning. MIT Press, Cambridge, MA, London, 2016. URL <http://www.deeplearningbook.org>.

J. C. Gower and G. J. S. Ross. Minimum spanning trees and single linkage cluster analysis. *Journal of the Royal Statistical Society: Series C (Applied Statistics)*, 18(1):54–64, 1969. URL <http://www.jstor.org/stable/2346439>.

B. Hammer. On the approximation capability of recurrent neural networks. *Neurocomputing*, 31(1-4):107–123, 2000. URL [http://doi.org/10.1016/S0925-2312\(99\)00174-5](http://doi.org/10.1016/S0925-2312(99)00174-5).

D. J. Higham and N. J. Higham. *MatLab Guide*. Siam, Philadelphia, PA, 3rd edition, 2017. URL <http://bookstore.siam.org/ot150/>.

S. Hochreiter and J. Schmidhuber. Long short-term memory. *Neural Computation*, 9(8):1735–1780, 1997. ISSN 0899-7667. URL <http://doi.org/10.1162/neco.1997.9.8.1735>.

R. A. Horn and C. R. Johnson. *Matrix Analysis*. Cambridge University Press, New York, NY, 2nd edition, 2013. URL <http://www.cse.zju.edu.cn/eclass/attachments/2015-10/01-1446086008-145421.pdf>.

K. Hornik. Approximation capabilities of multilayer feedforward networks. *Neural Networks*, 4(2):251–257, 1991. ISSN 0893-6080. URL [http://doi.org/10.1016/0893-6080\(91\)90009-T](http://doi.org/10.1016/0893-6080(91)90009-T).

H. Hu and G.-J. Qi. State-frequency memory recurrent neural networks. In D. Precup and Y. W. Teh, editors, *Proceedings of the 34th International Conference on Machine Learning*, volume 70 of *Proceedings of Machine Learning Research*, pages 1568–1577, Sydney, Australia, 2017. PMLR. URL <http://proceedings.mlr.press/v70/hu17c.html>.

R. J. Hyndman and Y. Khandakar. Automatic time series forecasting: The forecast package for R. *Journal of Statistical Software*, 27(3), 2008. URL <http://doi.org/10.18637/jss.v027.i03>.

R. J. Hyndman and G. Athanasopoulos. *Forecasting: principles and practices*. OTexts, Melbourne, Australia, 2013. URL <http://otexts.com/fpp2/>.

G. Indiveri, B. Linares-Barranco, T. Hamilton, A. van Schaik, R. Etienne-Cummings, T. Delbrück, S.-C. Liu, P. Dudek, P. Häfliger, S. Renaud, J. Schemmel, G. Cauwenberghs, J. Arthur, K. Hynna, F. Folowosele, S. Saighi, T. Serrano-Gotarredona, J. Wijekoon, Y. Wang, and K. Boahen. Neuromorphic silicon neuron circuits. *Frontiers in Neuroscience*, 5:73, 2011. ISSN 1662-453X. URL <http://www.frontiersin.org/article/10.3389/fnins.2011.00073>.

H. Jaeger. Echo state network. *Scholarpedia*, 2(9):2330, 2007. URL <http://doi.org/10.4249/scholarpedia.2330>. Revision #151757.

H. Jaeger. Controlling recurrent neural networks by conceptors. CoRR – Computing Research Repository abs/1403.3369, Cornell University Library, 2014. URL <http://arxiv.org/abs/1403.3369>.

H. Jaeger. Using conceptors to manage neural long-term memories for temporal patterns. *Journal of Machine Learning Research*, 18(1):387–429, 2017. URL <http://dl.acm.org/doi/abs/10.5555/3122009.3122022>.

H. Jaeger and H. Haas. Harnessing nonlinearity: Predicting chaotic systems and saving energy in wireless communication. *Science*, 2(304):78–80, 2004. URL <http://doi.org/10.1126/science.1091277>.

I. Jolliffe. Principal component analysis. In M. Lovric, editor, *International Encyclopedia of Statistical Science*, pages 1094–1096. Springer, Berlin, Heidelberg, 2011. ISBN 978-3-642-04898-2. URL [http://doi.org/10.1007/978-3-642-04898-2\\_455](http://doi.org/10.1007/978-3-642-04898-2_455).

H. Kitano, M. Asada, Y. Kuniyoshi, I. Noda, E. Osawa, and H. Matsubara. RoboCup: A challenge problem for AI. *AI Magazine*, 18(1):73–85, 1997. URL <http://www.aaai.org/ojs/index.php/aimagazine/article/view/1276/1177>.

D. Koryakin, J. Lohmann, and M. V. Butz. Balanced echo state networks. *Neural Networks*, 36:35–45, 2012. ISSN 0893-6080. URL <http://doi.org/10.1016/j.neunet.2012.08.008>.

S. Krause, O. Otto, and F. Stolzenburg. Fast classification learning with neural networks and conceptors for speech recognition and car driving maneuvers. In P. Chomphuwiiset, J. Kim, and P. Pawara, editors, *Proceedings of the 14th Multi-Disciplinary International Conference on Artificial Intelligence (MIWAI)*, LNAI 12832, pages 45–57. Springer Nature Switzerland, 2021. doi: 10.1007/978-3-030-80253-0\_5. URL [http://link.springer.com/chapter/10.1007/978-3-030-80253-0\\_5](http://link.springer.com/chapter/10.1007/978-3-030-80253-0_5).

R. Kruse, C. Borgelt, C. Braune, S. Mostaghim, and M. Steinbrecher. *Computational Intelligence. A Methodological Introduction*. Springer, London, 2nd edition, 2016. URL <http://link.springer.com/book/10.1007/978-1-4471-7296-3>.

N. Lee, T. Ajanthan, and P. H. S. Torr. SNIP: Single-shot network pruning based on connection sensitivity. In *International Conference on Learning Representations*, 2019. URL <http://arxiv.org/abs/1810.02340>.

Y. Liao and H. Li. Reservoir computing trend on software and hardware implementation. *Global Journal of Researches in Engineering (F)*, 17(5), 2017. URL <http://engineeringresearch.org/index.php/GJRE/article/download/1654/1585>.

Z. C. Lipton, J. Berkowitz, and C. Elkan. A critical review of recurrent neural networks for sequence learning. CoRR – Computing Research Repository abs/1506.00019, Cornell University Library, 2015. URL <http://arxiv.org/abs/1506.00019>.

S. Litz. Predicting stock prices using recurrent neural networks. WAIT – Wernigeröder Automatisierungs- und Informatiktexte 01/2020, Automation and Computer Sciences Department, Harz University of Applied Sciences, 2020. URL <http://dx.doi.org/10.25673/35875>. In German.

J. Liu, H. Lin, X. Liu, B. Xu, Y. Ren, Y. Diao, and L. Yang. Transformer-based capsule network for stock movement prediction. In *Proceedings of the First Workshop on Financial Technology and Natural Language Processing*, pages 66–73, Macao, China, 2019. URL <http://www.aclweb.org/anthology/W19-5511>.

W. Maass, T. Natschläger, and H. Markram. Real-time computing without stable states: A new framework for neural computation based on perturbations. *Neural Computation*, 14(11):2531–2560, 2002. URL <http://doi.org/10.1162/089976602760407955>.

G. Manjunath and H. Jaeger. Echo state property linked to an input: Exploring a fundamental characteristic of recurrent neural networks. *Neural Computation*, 25(3):671–696, 2013. URL [http://doi.org/10.1162/NECO\\_a\\_00411](http://doi.org/10.1162/NECO_a_00411). PMID: 23272918.

J. Martens and I. Sutskever. Learning recurrent neural networks with Hessian-free optimization. In *Proceedings of the 28th International Conference on Machine Learning*, pages 1033–1040, 2011. URL <http://dl.acm.org/doi/10.5555/3104482.3104612>.

S. Marzen. Difference between memory and prediction in linear recurrent networks. *Physical Review E*, 96(3):032308 [1–7], 2017. URL <http://doi.org/10.1103/PhysRevE.96.032308>.

C. Mead. Neuromorphic electronic systems. *Proceedings of the IEEE*, 78(10):1629–1636, Oct. 1990. URL <http://ieeexplore.ieee.org/document/58356>.

O. Michael, O. Obst, F. Schmidsberger, and F. Stolzenburg. Analysing soccer games with clustering and conceptors. In H. Akyama, O. Obst, C. Sammut, and F. Tonidandel, editors, *RoboCup 2017: Robot Soccer World Cup XXI. RoboCup International Symposium*, LNAI 11175, pages 120–131, Nagoya, Japan, 2018. Springer Nature Switzerland. URL [http://doi.org/10.1007/978-3-030-00308-1\\_10](http://doi.org/10.1007/978-3-030-00308-1_10).

O. Michael, O. Obst, F. Schmidsberger, and F. Stolzenburg. RoboCupSimData: Software and data for machine learning from RoboCup simulation league. In D. Holz, K. Genter, M. Saad, and O. von Stryk, editors, *RoboCup 2018: Robot Soccer World Cup XXII. RoboCup International Symposium*, LNAI 11374, pages 230–237, Montréal, Canada, 2019. Springer Nature Switzerland. URL [http://doi.org/10.1007/978-3-030-27544-0\\_19](http://doi.org/10.1007/978-3-030-27544-0_19).

P. Molchanov, A. Mallya, S. Tyree, I. Frosio, and J. Kautz. Importance estimation for neural network pruning. In *IEEE/CVF Conference on Computer Vision and Pattern Recognition (CVPR)*, pages 11256–11264, 2019. URL <http://doi.org/10.1109/CVPR.2019.01152>.

D. M. Q. Nelson, A. C. M. Pereira, and R. A. de Oliveira. Stock market’s price movement prediction with lstm neural networks. In *International joint conference on neural networks (IJCNN)*. IEEE, 2017. URL <http://doi.org/10.1109/IJCNN.2017.7966019>.

Y. Ollivier, C. Tallec, and G. Charpiat. Training recurrent networks online without backtracking. CoRR – Computing Research Repository abs/1507.07680, Cornell University Library, 2015. URL <http://arxiv.org/abs/1507.07680>.

H. Palangi, L. Deng, and R. K. Ward. Learning input and recurrent weight matrices in echo state networks. CoRR – Computing Research Repository abs/1311.2987, Cornell University Library, 2013. URL <http://arxiv.org/abs/1311.2987>.

L. Pasa and A. Sperduti. Pre-training of recurrent neural networks via linear autoencoders. In *Advances in Neural Information Processing Systems 27 (NIPS 2014)*, pages 3572–3580, 2014. URL <http://papers.nips.cc/paper/5271-pre-training-of-recurrent-neural-networks-via-linear-autoencoders>.

R. Pascanu, T. Mikolov, and Y. Bengio. On the difficulty of training recurrent neural networks. *Proceedings of the 30th International Conference on Machine Learning*, 28(3):1310–1318, 2013. URL <http://proceedings.mlr.press/v28/pascanu13.pdf>.

V. Pong, S. Gu, and S. Levine. Learning long-term dependencies with deep memory states. In *Lifelong Learning: A Reinforcement Learning Approach Workshop, International Conference on Machine Learning.*, 2017. URL <http://pdfs.semanticscholar.org/2e09/9bf26976e2334a9c4a2ad1aefc28cf83299b.pdf>.

M. Ragni and A. Klein. Predicting numbers: An AI approach to solving number series. In J. Bach and S. Edelkamp, editors, *KI 2011: Advances in Artificial Intelligence – Proceedings of the 34th Annual German Conference on Artificial Intelligence*, LNAI 7006, pages 255–259, Berlin, 2011. Springer. URL [http://doi.org/10.1007/978-3-642-24455-1\\_24](http://doi.org/10.1007/978-3-642-24455-1_24).

R. Reed. Pruning algorithms – a survey. *IEEE Transactions on Neural Networks*, 4(5):740–747, 1993. doi: 10.1109/72.248452. URL <http://ieeexplore.ieee.org/document/248452>.

M. Roondiwala, H. Patel, and S. Varma. Predicting stock prices using LSTM. *International Journal of Science and Research (IJSR)*, 6(4):1754–1756, 2017. URL <http://www.ijsr.net/archive/v6i4/ART20172755.pdf>.

J. Schmidhuber, D. Wierstra, M. Gagliolo, and F. Gomez. Training recurrent networks by Evolino. *Neural Computation*, 19:757–779, 2007. URL <http://doi.org/10.1162/neco.2007.19.3.757>.

D. Shah, H. Isah, and F. Zulkernine. Stock market analysis: A review and taxonomy of prediction techniques. *International Journal of Financial Studies*, 7(2), 2019. ISSN 2227-7072. doi: 10.3390/ijfs7020026. URL <http://www.mdpi.com/2227-7072/7/2/26>.

A. Sperduti. Exact solutions for recursive principal components analysis of sequences and trees. In S. D. Kollias, A. Stafylopatis, W. Duch, and E. Oja, editors, *Artificial Neural Networks – ICANN*, pages 349–356, Berlin, Heidelberg, 2006. Springer. ISBN 978-3-540-38627-8. URL [http://link.springer.com/chapter/10.1007/11840817\\_37](http://link.springer.com/chapter/10.1007/11840817_37).

F. Stolzenburg. Periodicity detection by neural transformation. In E. Van Dyck, editor, *ESCOM 2017 – 25th Anniversary Conference of the European Society for the Cognitive Sciences of Music*, pages 159–162, Ghent, Belgium, 2017. IPEM,

Ghent University. URL <http://www.escom2017.org/wp-content/uploads/2016/06/Stolzenburg-et-al.pdf>. Proceedings.

F. Stolzenburg, O. Michael, and O. Obst. The power of linear recurrent neural networks. In D. Brunner, H. Jaeger, S. Parkin, and G. Pipa, editors, *Cognitive Computing – Merging Concepts with Hardware*, Hannover, 2018. URL <http://cognitive-comp.org/#topics>. Received Prize for Most Technologically Feasible Poster Contribution.

S. H. Strogatz. *Nonlinear Dynamics and Chaos. With Applications to Physics, Biology, Chemistry, and Engineering*. CRC Press, Boca Raton, FL, 2nd edition, 2015. URL <http://doi.org/10.1201/9780429492563>.

R. S. Sutton and A. G. Barto. *Reinforcement Learning: An Introduction*. MIT Press, 2nd edition, 2018. URL <http://incompleteideas.net/book/the-book.html>.

T. Tao, V. Vu, and M. Krishnapur. Random matrices: Universality of ESDs and the circular law. *The Annals of Probability*, 38(5):2023–2065, 2010. URL <http://projecteuclid.org/euclid.aop/1282053780>.

P. Tiňo. Asymptotic Fisher memory of randomized linear symmetric echo state networks. *Neurocomputing*, 298:4–8, 2018. URL <http://doi.org/10.1016/j.neucom.2017.11.076>.

A. R. Voelker, I. Kajić, and C. Eliasmith. Legendre memory units: Continuous-time representation in recurrent neural networks. In *Advances in Neural Information Processing Systems 32 (NeurIPS 2019)*, Vancouver, Canada, 2019. URL <http://proceedings.neurips.cc/paper/2019/file/952285b9b7e7a1be5aa7849f32ffff05-Paper.pdf>.

O. L. White, D. D. Lee, and H. Sompolinsky. Short-term memory in orthogonal neural networks. *Physical Review Letters*, 92(14):148102, 1994. URL <http://journals.aps.org/prl/abstract/10.1103/PhysRevLett.92.148102>.

Y. Xue, L. Yang, and S. Haykin. Decoupled echo state networks with lateral inhibition. *Neural Networks*, 20(3):365–376, 2007. URL <http://doi.org/10.1016/j.neunet.2007.04.014>.